TECHNICAL AND VOCATIONAL TRAINING INSTITUTE (TVTI)

SCHOOL OF GRADUATE STUDENT
FACULTY OF ELECTRICAL AND ELECTRONICS TECHNOLOGY AND INFORMATION AND COMMUNICATION TECHNOLOGY (DEPARTMENT OF ELECTRICAL AND ELECTRONICS TECHNOLOGY)

Model Predictive Speed Control of Permanent Magnet Synchronous Motor

Msc thesis for the partial fulfillment of

Master of science in Electrical automation and control technology management

By,

Ahmed Eshete Yesuf (MTR/435/13)

Supervisor,

Dr.Chala Merga

AUGUST 2022

Addis Ababa,Ethiopia

Model Predictive Speed Control of Permanent Magnet Synchronous Motor

A Thesis submitted to

TECHNICAL AND VOCATIONAL TRAINING INSTITUTE (TVTI)
FACULTY OF ELECTRICAL AND ELECTRONICS TECHNOLOGY AND INFORMATION AND COMMUNICATION TECHNOLOGY (DEPARTMENT OF ELECTRICAL AND ELECTRONICS TECHNOLOGY)

In partial fulfillment for the Degree

MASTER OF SCIENCE *in* ELECTRICAL AUTOMATION AND CONTROL TECHNOLOGY MANAGEMENT

By,

Ahmed Eshete Yesuf MTR/435/13

Supervisor,

Dr.Chala Merga

DECLARATION

I hereby declare that the work which is being presented in this thesis entitled ”Model Predictive speed control of permanent magnet synchronous motor” is the original work of my own, has not been presented for a masters thesis in this or other universities and all sources of materials used for this thesis work have been fully acknowledged.

Name: Ahmed Eshete Yesuf

Signature: _____

Place: Addis Ababa

Date of Submission:_____

This thesis proposal has been submitted for examination with my approval as a TVTI advisor.

Dr. Chala Merga _____

Advisor Name Signature Date

TECHNICAL AND VOCATIONAL TRAINING INSTITUTE (TVTI)
FACULTY OF ELECTRICAL AND ELECTRONICS TECHNOLOGY AND INFORMATION AND COMMUNICATION TECHNOLOGY
(DEPARTMENT OF ELECTRICAL AND ELECTRONICS TECHNOLOGY)

Thesis on

Model Predictive Speed Control Of Permanent Magnet Synchronous Motor

By,

Ahmed Eshete Yesuf (MTR /435/13)

APPROVED BY THESIS ADVISORY COMMITTEE

Name of the advisor Dr.Chala Merga	signature	Date 03. September. 2022
Name of the Examiner Internal Dr. Yohans	signature	Date 05 Sep 2022
Name of the Examiner External Dr. Mengesha Mamo	signature	Date September 2, 2022
Name of the Examiner Internal	signature	Date
Name of the Chairperson Zemenu Tamir	signature	Date 05/09/22

ACKNOWLEDGEMENT

First and foremost, we would like to express our deep whole hearted gratitude to my advisor Dr Chala Merga for for involvement their unreserved skill, expertise, and experience. His advice and assistance were essential components of the task. I am also grateful to My wife for her helping optimistically. To justify it, it is beyond a word to explain the way he guides us, the way he shares us his experience that couldn't be explained only imprinted in my mind. My appreciation also extends to my parents and relatives who support and encourage us to complete this thesis in particular and the society in general. At last but not least, to start and to complete every activity, it is up on him, since my effort is blessed I am lucky, as a result it becomes tangible now and tomorrow it may be a vital ingredient for further implementation to simplify life, for all thanks for alah!

ABSTRACT

The PMSM system is a challenging, time-varying, nonlinear system. Various control methods have already been used to improve the PMSM's performance. The precise feedback linear control approach, which converts the novel nonlinear model into a linear model by suitable harmonize translation, is a logical choice given that the machine's dynamic model is nonlinear. This thesis presents new findings on the application of model predictive speed control of a permanent magnet synchronous motor, with the design based on a linearized state-space representation of the nonlinear model that describes the dynamics. The integral action used by the model predictive controller results in zero steady-state error and load torque disturbance rejection. The MPC is then compared to a standard approach, namely a Proportional Integral (PI) speed controller. The effectiveness of the approach is demonstrated by Simulink simulation results.

Keywords*: PMSM , PI, MPC, speed tracking, vector control*

TABLE OF CONTENTS

LIST OF FIGURES

LIST OF TABLES

ABBREVIATIONS

DC	Direct Current
DTC	Direct Torque Control
EMF	Electro Motive Force
FOC	Field Oriented Control
IM	Induction Motor
LPF	Low Pass Filter
LTID	Load Torque Identification
MIMO	Multiple-Input, Multiple-Output
PI	Proportional Integral
PLL	Phase-Locked Loop
PMSM	Permanent Magnet Synchronous Motor
PWM	Pulse Width Modulation
RPM	Round Per Minute
SVD	Singular Value Decomposition
SVM	Space Vector Modulation
VSI	Voltage Source Inverter
VSD	Variable Speed Drive
HPVSD	High-Performance Variable-Speed Drives

CHAPTER ONE

1 INTRODUCTION

1.1 Background

For a variety of uses in industry, the home, and transportation, modern permanent magnet synchronous machines (PMSMs) are gaining popularity. Due to the worldwide drift toward vitality preservation, there's an expanding require for electrical drives that are solid, high-performance, and energy-efficient. PMSMs are the perfect choices since of their amazing effectiveness, tall yield control per mass and volume, and extraordinary energetic reaction. Due to their distinct advantages of high efficiency, high power density, and a wide constant power region [1]. PMSM systems are increasingly being used in many industrial applications, including home appliances [2,3]. Systems for electric-drive vehicles and wind energy conversion (WECSs) [4]. PMSMs have become more appealing and competitive as the cost of permanent magnet synchronous motor materials has decreased and Control methods have evolved [5].

In recent years, a wide range of VSD topologies and techniques for permanent magnet synchronous motor have been carefully examined and documented. The most popular control methods are field oriented control (FOC) and direct torque control (DTC) [6]. Numerous solutions have been proposed in the literature to address these issues. Some of them implement DTC using space vector modulation, sometimes known as SVM-DTC. A traditional DTC's Switching table only has a limited amount of voltage vectors with specified amplitudes and positions. Using the SVM implementation, a voltage vector of any amplitude and location can be produced [8]. This allows for more precise torque and flux generation using SVM-DTC. SVM has the additional benefit of requiring less frequent sampling than traditional DTC. The academic and industrial worlds have recently been more familiar with model predictive control (MPC)[9]. To account for the discrete nature of power converters, predictive control algorithms take the converter and the motor into consideration as a whole.Depending on the kind of predictive control being employed, there are differences in the quantity of applied vectors, the vector selection process, and the predictive horizon.

1.2 Statement of the Problem

In a variety of industrial applications permanent magnet synchronous motors are used more commonly in HPVSD. This is due, among other things, to the PMSM's excellent efficiency, compactness, high torque to inertia ratio, quick dynamic response, simple modeling and control, and maintenance-free operation. Due to the correlation between the electrical quantities, in particular the d and q currents, and the motor speed, the model based of a PMSM is extremely nonlinear. Various control methods have already been used to improve the PMSM's performance. The precise feedback linear control approach, which converts the novel nonlinear model into a linear model by suitable harmonize translation, is a logical choice given that the machine's dynamic model is nonlinear. But because some of the variables in the equations will change, it's possible that the dynamics of synchronous motors as a whole are not fully understood. For instance, if the temperature changes, the resistance and inductance will change. As a result, parameter uncertainties affect the equations of motion and the feedback linearization technique can only partially erase nonlinearities. Thus, one of the main objectives of the control design is to create a strong controller that assures noble dynamic performances in the face of parameter uncertainty and disturbance. In order to achieve high dynamic performance on PMSMs and actual rotor position, variable voltage and variable frequency operation must be carried out by monitoring rotational speed and stator currents via mechanical sensors and returning them to the controllers. When compared to The significant improvements in system efficiency and performance that sensor-based PMSMs bring, the additional sensors and timing hardware needed to build them are affordable. Rotor position information that is erroneous not only affects control performance but also makes the control system unstable. Sliding mode control is additionally recognized as a reliable method for resolving nonlinear system control issues. It is possible to ensure robustness characteristics against a variety of uncertainties, including parameter alterations and load torque disturbances. MPC is based on finite-horizon iterative optimization of system model behavior. The model nonlinearities in an adaptive EMPC scheme are brought on by the product of the rotor flux or d-axis current with speed. When utilized for speed control, a cascade MPC offers the best dynamic performance while allowing torque (currents) to be regulated to the highest permissible value.

1.3 Objective

1.3.1 General Objective

The primary goal of this thesis is to design and simulate a model predictive speed control for a permanent magnet synchronous motor.

1.3.2 Specific Objective

This study seeks to develop a system that will address the following:

- To study the permanent magnet synchronous motors mathematical model.
- To model and design speed controller of the PMSM using model predictive control
- To analyze the performance of the controller under various load conditions.
- To simulate the system using MATLAB/SIMULINK.

1.4 Methodology

The following tasks are included in the methodology of this thesis for each specific objective. The first step is to perform a study of the literature in which all relevant theoretical data regarding the PMSM drive is obtained and earlier, comparable studies are contrasted. The PM motor driving theory's features and modeling are then investigated. The nonlinear dynamic mode of the PMSM drive serves as the foundation for the development of a model predictive controller control law. Then, utilizing vector control on MATLAB/Simulink, the space vector approach is employed to simulate speed control and load torque tracking of the motor.

1.5 Scope and Limitations

The goal of the thesis is to research, model, and develop a speed control strategy for a permanent magnet synchronous motor using a mechanical position/speed sensor to measure the rotor's instantaneous mechanical position/speed. The inaccessibility of the mechanical position/speed sensor is another drawback. The aim of this thesis is to design and simulate PMSM drive systems based on MPC. The following will be included in the project's scope:

- Modeling a (PMSM) is implemented using mathematical modeling in the MATLAB Simulink software.
- To control PMSM parameters, create a PMSM drive system based on MPC. The predictive controller forecasts the system's future behavior and uses that information to control the system's parameters.

1.6 Significance of Study

The main contribution of this paper is the introduction of a new Model Predictive Control-based control scheme for permanent magnet drives. The qualitative approach was founded on a model example that did not include any quantitative criteria. This controller exhibits good dynamical performance for all working points, including zero speed. It is worth noting that the dq model for control signal prediction determines the type of control, which is similar to vector control. The benefits of the proposed MPC algorithm in high dynamic systems are demonstrated. The algorithm is strongly recommended for control that requires rapid desired speed changes. Currently, there are investigations underway that could lead to real-world implementation.

1.7 Thesis Outline

Six chapters make up this thesis. The overview of the PMSM speed control in the first chapter covers the background, a problem statement, relevance, study objective,scope,and limits. the various PMSM control theory strategies are discussed in chapter two, along with a survey of the literature on PMSM speed control. The third chapter discusses system modeling, design, analysis, and implementation. The fourth chapter describes the standardized controller method, as well as the controller and observer tuning processes. Chapter five presents and discusses simulation results. The chapter also discusses the contributions of the thesis work. Chapter six concludes with recommendations and findings.

CHAPTER TWO

2 LITERATURE REVIEW

According to F. Genduso,R. Miceli, C. Rando and G.R. Galluzzo, the back EMF estimate method is perhaps the most popular approach to sensorless PMSM management [10]. It is straightforward, easy to calculate, and effective in high-speed control applications, but a well-known drawback of this kind of approach is that the back-EMF is rotor speed-dependent. Since the back-EMF is so modest at low speeds, reliable estimation is challenging [11, 12]. Other drawbacks of the back EMF estimation method include sensitivity to parameter uncertainties, measurement noise, and inverter irregularities [13]. The system speed is also controlled by the PI controller, which is affected by system parameter variation, making it difficult to tune the controller parameters [14] to improve system performance.

According to J. K. J. Kang, B. H. B. Hu, H. L. H. Liu and G. X. G. Xu [15] Provides extensive Another method for estimating PMSM rotor speed is the kalman filter. The kalman filteris a state observer that calculates the states of a dynamic linear system using least-squares optimization. The EKF is predicated on the idea that system noise and measurement errors are both zero-mean white Gaussian noise. One disadvantage of this system is that it only considers estimation model inaccuracies but not speed controller performance. Another disadvantage of EKF applications for PMSM speed estimation is the high processor requirements.

According to J. Son and J. Lee [16] Proposes a sensorless speed control strategy for a permanent-magnet synchronous motor (PMSM) based on a new sliding-mode observer (SMO) that uses a sigmoidal function as a switching function with variable boundary layers rather than a discontinuous signum function. In a conventional sliding-mode observer, a low pass filter causes a time delay (which uses a signum function). Because of its simplicity, the Sliding Mode Observer (SMO) is widely used. Because it is a back-EMF method, it has the obvious problems of standstill and low speed estimation. However, the SMO appears to outperform most other back-EMF estimation methods, and its simplicity makes it appealing (feasible). Despite the fact that the SMO is widely used due to its robustness against parameter variations and disturbances, the high frequency switching to the sliding surface causes high frequency noise in the system dynamics. This increases the estimation's constant error. The chattering effect is this phenomenon, and it is a well-known flaw in the SMO estimate method. [16, 17]. The author

also only considers the performance of the speed estimation method, not the performance of the speed controller when system parameters are changed.

According to Mahlet Legesse [18] A traditional PI speed controller's performance is impacted when the system parameters vary due to internal and external circumstances since the controller settings are dependent on the system parameters. It was suggested that this issue could be resolved by adopting a sensor-based online tweaking of PI speed controller parameters for a wide speed range and various load disturbances. However, the speed sensor raises the system cost, and the controller performance rises as the number of fuzzy rules increases, making the control algorithm more complex. Additionally, fuzzy logic controller design necessitates expert knowledge for system parameter changes, making controller design difficult.

According to Derege Eskezia [19] presents a reliable, low chattering-effect higher order sliding mode controller for PMSM that controls the proper reference speed. Variations in load torque and other factors have no impact on the proposed drive's speed response. The developed controller also performs effectively when the reference speed is changed. The main disadvantage of this system was that the chattering effect of the speed controller output remained even after it was minimized, and the speed and position information for FOC-based control of the PMSM drive was obtained by using a mechanical sensor, which increased the cost of the system and decreased its reliability in harsh environments.

The Neural network observer in [20] paper is designed to estimate speed and position using direct and quadrature current and voltage components. The proposed Neural Network Observer design provides accurate speed estimation and benefits from reduced mathematical computations. It also includes the SMC controller; the drive provides improved performance regardless of load variations. Despite the fact that the system performs well under variable load conditions and that speed estimation is robust to parameter uncertainty, it requires a long processing time due to the neural network learning rate, which is very complex and difficult to implement. Due to the use of SMC for the drives, there is also chattering on the speed controller output.

According to Ji-Hoon Jang[21] presents a new sensorless control method for an SPMSM based on a high-frequency impedance difference using a high-frequency voltage signal injection method. The flux of the permanent magnet in the SPMSM causes saturation of the stator core around the q-axis winding. This increases the motor's magnetic saliency. The rotor position is

encoded in this magnetic saliency. In order to detect magnetic saliency and estimate rotor position, a high-frequency voltage signal is injected into the motor.

2.1 Summary of Literature Review

Electrical drives have been widely used in a variety of industry applications in recent decades. However, the PMSM drive has several advantages that set it apart from other electrical motor drives. Furthermore, PMSM offers additional benefits such as high efficiency, low rotor losses, high power density, simple structure, and small size, which reduces maintenance costs. PMSM is an alternating current motor that is powered by alternating current. As a result, an inverter is required to convert the DC source power to AC power and feed it to the PMSM. However, due to its highly nonlinear nature, it has an unstable response and thus provides a high performance. However, in order to provide a more accurate response and a high performance, an advanced control strategy must be used to control the input power of the PMSM. Additionally, the output of the inverter will require regulation Voltage,Current and Frequency. Different control techniques have been used to manage the high-performance system. Vector controllers, FOC, and DTC are examples. However, MPC has numerous advantages that make it ideal for controlling the PMSM drive system. The MPC principle is intuitive and simple to understand; it can be applied to a variety of systems; constraints and nonlinearities can be easily included, reducing complexity; multivariable cases can be easily considered, and the resulting controller is simple to apply. In comparison to the other methods, it necessitates a greater number of calculations. MPC functions are based on the prediction of a system's future behavior and provide the best action for the requirement.

Table 2.1 Summary of Literature Review

Authors	Title	Key findings	Gaps
F. Genduso, R. Miceli, C. Rando and G. R. Galluzzo 2009 in [10]	Back-EMF Sensorless Control Algorithm forHigh Dynamics Performances PMSM	It is simple to estimate the speed. It performs admirably at high speed control.	-It is impossible to estimate at low and standstill speeds. -Sensitivity to parameter change. -It employs a PI speed controller.
J. K. J. Kang, B. H. B. Hu, H. L. H. Liu,and G. X. G.Xu 2009 in [15]	Sensorless Control of Permanent Magnet Synchronous Motor Based on Extended Kalman Filter	-It can estimate speed under all operating conditions..	-It does not take into account speed control performance (PI controller is used) -High processor requirements
J. Son and J.Lee 2011 in [16]	A High-Speed Sliding-Mode Observer for the Sensorless Speed Controlof a PMSM	-It is simple to design -It is resistant to parameter variation -Accurate speed estimation at high speeds	-Standstill and low speed estimation issues The chattering effect The issue of time lag. -It employs a PI speed controller.
Mahlet Legesse 2011 in [18]	Speed controller of vector control PMSM Drive by Fuzzy Logic-PI control	-Using FLC, online tuning of PI speed controller parameters. -It performs well with parameter variation and variable load torque.	-It is a sensor-based speed controller -FLC Speed controller necessitated expert knowledge - A more complex control algorithm.

Derege Eskezia 2017 in [19]	Speed Controller Of PMSM Higher Order Sliding Mode Controling	- Variations in load torque and characteristics have no impact on the proposed drive's speed response.	-The output of the speed control chatters. -The sensor-derived speed signal.
Syed Abdul Rahman Kashif and Muhammad Asghar Saqib 2016 in [20]	Sensorless Control of a Permanent Magnet Synchronous Motor Using Artificial Neural Network Based Estimator	-A learn-based system for speed estimation that is easy to train and independent of motor parameters. Powerful speed controller	-A learn-based system for speed estimation that is easy to train and independent of motor parameters. Powerful speed controller
Ji-Hoon Jang 2003 in [21]	Sensorless Drive of Surface-Mounted Permanent-MagnetMotor by High- Frequency Signal Injection Based on Magnetic Saliency	-Best at low speed estimation - And independent of motor parameter variation	-Difficult to implement -Noise at medium and High speed conditions, -it uses traditional PIspeed controller

CHAPTER THREE

3 MODELING AND DESIGN OF A PMSM SPEEDCORDER

3.1 Introduction

The rotating velocity and d-q axis current product terms in the dynamic model of a PMSM are highly connected, making it a nonlinear time-varying system with MIMO. To achieve precise control performance, the system needs to be linearized and decoupled. Magnet motor performance has recently been improved by using a number of control algorithms. a logical choice given that the machine's dynamic model is nonlinear. But because some of the variables in the equations will change, it's possible that the dynamics of synchronous motors as a whole are not fully understood. For instance, if the temperature changes, the resistance and inductance will change. As a result, parameter uncertainties affect the equations of motion and the feedback linearization technique can only partially erase nonlinearities. An important objective of the control design is hence the creation of a robust controller that guarantees high dynamic performances in the face of parameter uncertainty and disturbance[22]. The detailed mathematical modeling of a permanent magnet synchronous motor is covered in this chapter.

3.2 Mathematical Model of PMSM

A permanent magnet rotor and an electromagnetic stator power PMSMs. Instead of an alternating current, as in DC motors, permanent magnets produce the magnetic flux that powers the rotor. Brushless motors do not require mechanical contact between the stator and rotor because no current is applied to the rotor. The rotor of a PMSM can be built in a variety of ways. The number of magnets or pole pairs used is the most evident design strategy. the motor's synchronous speed and torque production at a given current are influenced by the number of pole pairs. The rotor magnets can also be positioned inside the iron core or on top of the iron core (surface mounted PMSM) (internal mounted PMSM). The kind of installation has an impact on the inductance that the rotor produces. Generally speaking, rotor position affects the stator winding inductance. The fluctuating inductance causes the winding's current responsiveness to vary. The stator self-inductances are unaffected by the placement of the rotor if the rotor is believed to be surface mounted, as is typical with brushless motors.

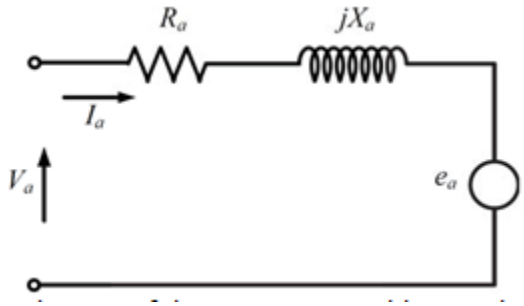

Figure 3.1 Diagram of the SM's comparable per-phase circuit

The voltage equation for the stator phase is as follows:

$$u_s = R_s i_s + \frac{d\psi_s}{dt} \tag{3.1}$$

The PMSM model can be derived in a stationary reference frame by presuming that the three phase Is and the spinning magnet both contribute to the flux linkage.

$$\begin{bmatrix} v_a \\ v_b \\ v_c \end{bmatrix} = R_s \begin{bmatrix} i_a \\ i_b \\ i_c \end{bmatrix} + \begin{bmatrix} L_{aa} & L_{ab} & L_{ac} \\ L_{ba} & L_{bb} & L_{bc} \\ L_{ca} & L_{bc} & L_{cc} \end{bmatrix} \frac{d}{dt} \begin{bmatrix} i_a \\ i_b \\ i_c \end{bmatrix} + \frac{\partial}{\partial \theta} \begin{bmatrix} \psi_a \\ \psi_b \\ \psi_c \end{bmatrix} \omega_e \tag{3.2}$$

Where v_a, v_b and v_c are three phase voltage,

i_a, i_b and i_c the three phase current, ψ_a, ψ_b and ψ_c the three flux linkage and

$$\begin{matrix} L_{aa} & L_{ab} & L_{ac} \\ L_{ba} & L_{bb} & L_{bc} \\ L_{ca} & L_{bc} & L_{cc} \end{matrix}$$ the inductance matrix.

Equation (3.2) is frequently used to calculate the machine's back emf, and it has been found that the emf values are proportional to the rotating speed. The two-phase orthogonal reference frame in stationary and rotation are developed to decouple flux and torque control (α - β and *d*-*q* reference frames).

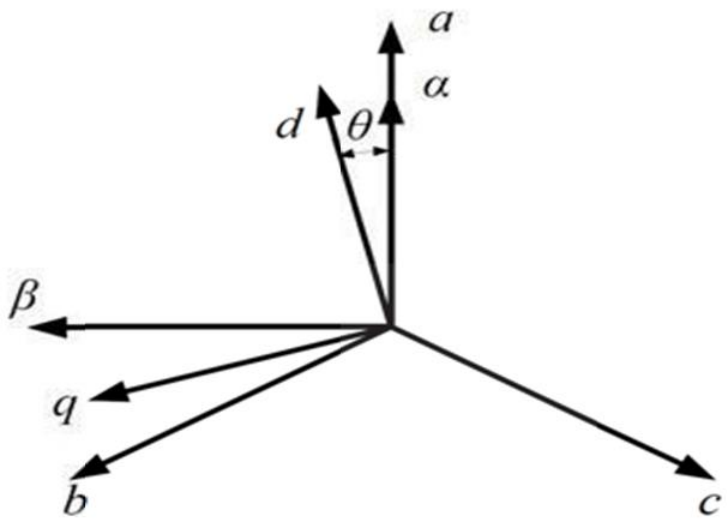

Figure 3.2 Relationship between different reference frames

The variables are transformed between these reference frames using the park and Clarke transformations, which are indicated as follows.

$$\begin{bmatrix}\psi_\alpha \\ \psi_\beta\end{bmatrix} = \sqrt{\frac{2}{3}}\begin{bmatrix}1 & -\frac{1}{2} & -\frac{1}{2} \\ 0 & \frac{\sqrt{3}}{2} & -\frac{\sqrt{3}}{2}\end{bmatrix}\begin{bmatrix}\psi_a \\ \psi_b \\ \psi_c\end{bmatrix} \tag{3.3}$$

$$\begin{bmatrix}\psi_d \\ \psi_d\end{bmatrix} = \sqrt{\frac{2}{3}}\begin{bmatrix}\cos\theta & \cos(\theta-\frac{2\pi}{3}) & \cos(\theta+\frac{2\pi}{3}) \\ -\sin\theta & -\sin(\theta-\frac{2\pi}{3}) & -\sin(\theta+\frac{2\pi}{3})\end{bmatrix}\begin{bmatrix}\psi_a \\ \psi_b \\ \psi_c\end{bmatrix} \tag{3.4}$$

As a result, the machine electrical variables could be expressed in stationary form used *d-q* Reference frame variables.the *Vp*,current,and flux linkage α could be written as:

$$\begin{cases} i_a = \sqrt{\frac{2}{3}}\left(i_d cos\theta - i_q sin\theta\right) \\ u_a = \sqrt{\frac{2}{3}}\left(u_d cos\theta - u_q sin\theta\right) \\ \psi_a = \sqrt{\frac{2}{3}}\left(\psi_d cos\theta - \psi_q sin\theta\right) \end{cases} \tag{3.5}$$

By substituting (3.5) into (3.1), a simplified expression can be:

$$(\frac{d\psi_d}{dt} - \psi_q\frac{d\theta}{dt} + R_s i_d - u_d)\cos\theta + (-\frac{d\psi_q}{dt} - \psi_d\frac{d\theta}{dt} - R_s i_q + u_q)\sin\theta = 0 \tag{3.6}$$

This equation should hold true for any value of ş. As a result, the voltage equations for the d-q axes shown below are always valid.

$$\begin{cases} u_d = R_s i_d + \dfrac{d\psi_d}{dt} - \psi_d \dfrac{d\theta}{dt} \\ u_q = R_s i_q + \dfrac{d\psi_q}{dt} - \psi_q \dfrac{d\theta}{dt} \end{cases} \tag{3.7}$$

The d- and q-axes flow linkages in the basic machine model are often specified as follows:

$$\begin{cases} \psi_d = L_d i_d + \psi_f \\ \psi_q = L_d i_q \end{cases} \tag{3.8}$$

Where W is the flux linkage created by the permanent magnet, and Lq and Lq are the d- and q-axis inductances, respectively. It is discovered that the only element contributing to the development of the q-axis flux linkag is the q-axis Is. The permanent magnet on the rotor and the d-axis stator current both contribute to the flux linkage along the d-axis. The comparable circuit for the electrical model in (3.7), which is rewrittens as in Figure 3.3, is shown in the d-q reference frame (3.9).

$$\begin{cases} u_d = R_s i_d + L_d \dfrac{di_d}{dt} - \omega L_q i_q \\ u_q = R_s i_q + L_q \dfrac{di_q}{dt} + \omega_e L_d i_q + \omega_e \psi_f \end{cases} \tag{3.9}$$

The three-phase terminal voltages and currents can be utilized to display the machine's total input power when it is being used as a motor. The d-q rotating reference frame can then be used with these quantities.

$$P_{in} = u_a i_a + u_b i_b + u_c i_c \tag{3.10}$$

$$P_{in} = \frac{3}{2}(u_d i_d + u_q i_q) \tag{3.11}$$

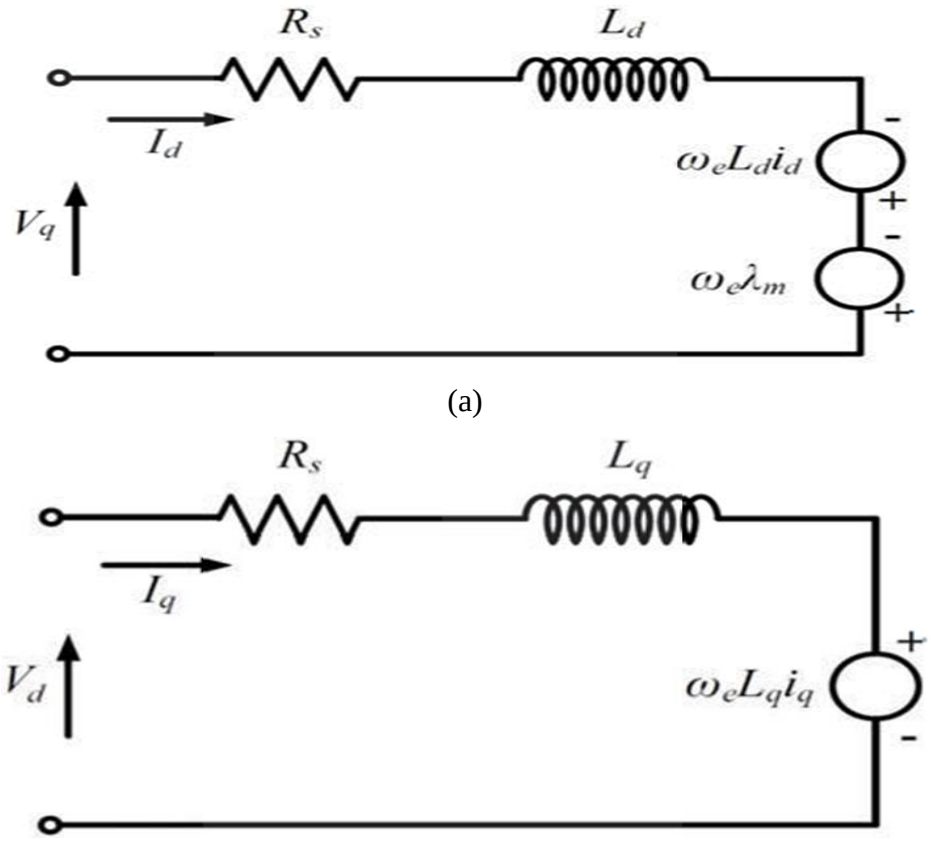

Figure 3.3 In (a) d and (b) d-axis, the PMSM equivalent circuit

By switch equation (3.9) for equation (3.8), the input total power expression can be generated as a combined purpose of the d-q axis currents (3.11).

$$P_{in} = [R_s(i_d^2 + i_q^2) + i_q \frac{d\psi_q}{dt} + i_d \frac{d\psi_d}{dt} + \omega_e(\psi_q i_q - \psi_d i_d)] \tag{3.12}$$

The electromechanical power becomes: when the terms for copper losses and magnetic energy variation are removed.

$$P_{em} = \frac{3}{2}\frac{p\omega_r}{2}(\psi_q i_q - \psi_d i_d) \tag{3.13}$$

when the rotor's electrical speed is changed to its mechanical speed.

$$\omega_e = \frac{p}{2}\omega_r \tag{3.14}$$

Where p is the number of poles For the mechanical equations of the model, we have.

$$T_e = T_L + J\frac{d\omega_r}{dt} + F.\omega_r \tag{3.15}$$

Where T_L the load torque applied on the rotor shaft, J the inertia of the motor and F the shadt friction coefficient. One can calculate the electromagnetic torque expression by dividing the electromagnetic power by the rotor mechanical speed. Because the PMSMs lack damping windings, damping effects are ignored in this model. The electromagnetic torque is denoted by:

$$T_e = \frac{3}{2}p(\psi_d i_q - \psi_q i_q) \tag{3.16}$$

By substituting (3.8) into (3.16)

$$\begin{aligned} T_e &= \frac{3}{2}p[\psi_f i_q + (L_d - L_q) i_d i_q] \\ &= \frac{3p|\psi_s|}{4L_d L_q}[2\psi_f L_q \sin\delta + |\psi_s|(L_d - L_q)\sin 2\delta] \end{aligned} \tag{3.17}$$

Where δ is the electrical angle between stator and rotor flux vectors.

The electromagnetic torque, as shown, is made up of two components: the rotor saliency-induced reluctance torque and the permanent-magnet torque. The d- and q-axis inductances of a surface-mounted PMSM without saliency are equal to the synchronous inductance, i.e. $L_d = L_q = L_s$. The torque is simplified because it excludes the reluctance torque.

$$T_e = \frac{3}{2}p\psi_f i_q = \frac{3}{2}p\frac{\psi_f |\psi_s|}{L_s}\sin\delta \tag{3.18}$$

Similarly, the voltage and stator-flux equations can be simplified. They can be expressed using a complex vector in the stationary frame (the components denoted by $\alpha\beta$) as:

$$u_s = R_s i_s + \frac{d\psi_s}{dt} \tag{3.19}$$

$$\psi_s = L_s i_s + \psi_r \tag{3.20}$$

Where $\psi_r = \psi_f e^{j\theta r}$ and the torque in the stationary frame is said as:

$$T_e = \frac{3}{2}p\psi_s x i_s = \frac{3}{2}p(\psi_{sa} i_{s\beta} - \psi_{s\beta} i_{sa}) \tag{3.21}$$

Pushing the d-axis current towards zero to produce the most torque while avoiding reluctance effects and torque ripple, vector control guarantees that the i_s space vector only contains a quadrature element [25].

By setting $\frac{d\theta}{dt} = \omega$ We can obtain the PMSM's state equation using the formula below:

$$\begin{bmatrix} \frac{d\theta}{dt} \\ \frac{di_d}{dt} \\ \frac{di_q}{dt} \end{bmatrix} = \begin{bmatrix} -\frac{R}{L} i_d + \omega i_q + \frac{V_d}{L} \\ -\frac{R}{L} i_q - \omega i_d - \frac{\lambda_m}{L} \omega + \frac{u_q}{L} \end{bmatrix} \tag{3.22}$$

Now $\omega = P\omega_r$ and $\omega = P\theta_r$ The mechanical motion of the PMSM is expressed by the stae equation as

$$\begin{bmatrix} \frac{d\theta_r}{dt} \\ \frac{d\omega_r}{dt} \\ \frac{di_d}{dt} \\ \frac{di_q}{dt} \end{bmatrix} = \begin{bmatrix} \omega \\ \frac{3p}{2J} \lambda_m i_q - \frac{B}{J} \omega_r - \frac{Tl}{J} \\ -\frac{R}{L} i_d + P\omega_r i_q + \frac{V_d}{L} \\ -\frac{R}{L} i_q - p\omega_r i_d - P\frac{\lambda_m}{L} \omega_r + \frac{u_q}{L} \end{bmatrix} \tag{3.23}$$

Where, u_d, u_q and i_q i_d are the voltage and current components of the d- and q-axes.

The equation (3.23) shows that the PMSM is a multi-variable, coupled, nonlinear system with time variations.

$$\frac{d}{dt} \begin{bmatrix} i_d \\ i_q \\ \omega_r \\ \theta_r \end{bmatrix} = \begin{bmatrix} -\frac{R}{L} & p\omega_r & 0 & 0 \\ -P\omega_r & -\frac{R}{L} & -P\frac{\lambda_m}{L} & 0 \\ -P\omega_r & \frac{3P}{2J}\lambda_m & -\frac{B}{J} & 0 \\ 0 & 0 & 1 & 0 \end{bmatrix} \begin{bmatrix} i_d \\ i_q \\ \omega_r \\ \theta_r \end{bmatrix} + \begin{bmatrix} \frac{1}{L} & 0 \\ 0 & \frac{1}{L} \\ 0 & 0 \\ 0 & 0 \end{bmatrix} \begin{bmatrix} u_d \\ u_q \end{bmatrix} \tag{3.24}$$

$$\begin{bmatrix} i_d \\ i_q \end{bmatrix} = \begin{bmatrix} 1 & 0 & 0 & 0 \\ 0 & 1 & 0 & 0 \end{bmatrix} \begin{bmatrix} i_d \\ i_q \\ \omega_r \\ \theta_r \end{bmatrix} \tag{3.25}$$

From the (3.25) it can be seen that PMSM a MIMO and coupled non LTI system.

For considering speed Model Predictive Control vector x choosed:

$$\underline{x}_{MPC} = \left[i_d \; i_q \; \omega_r \; \theta \right] \tag{3.26}$$

State matrices would be simplified in turn. Torque at load T_{load} is considered a known disturbance. The method of control is determined by the appearance of the decoupled *dq*-axis model. The rotor reference frame's two phase voltages *Vd* and *Vq* are then transformed into three phase stator reference voltages Va, Vb, and Vc, which serve as modulating voltages for the modulator, which employs the space vector pulse width modulation (SVPWM) scheme. The traditional two-level voltage source inverter is powered by the modulator output, which comes in the form of pulses, and anti-parallel diodes serve as switches (VSI).

3.3 SVPWM for Inverter Fed PMSM

The space vector pulse width modulation (SVPWM) method is a sophisticated computation-intensive PWM method that may be the best of all PWM methods for variable frequency drive applications [2], [6]. It has found widespread application in recent years due to its superior performance characteristics. The prospect of improved bus voltage consumption and the decrease of overall harmonic distortion brought on by the PWM algorithm's quick switching are two of SVPWM's main benefits [1], [2]. As shown in Figure 3.6, The positive and negative terminals of the DC bus voltage are connected to the phases of the motor through the legs of the three phase inverter.

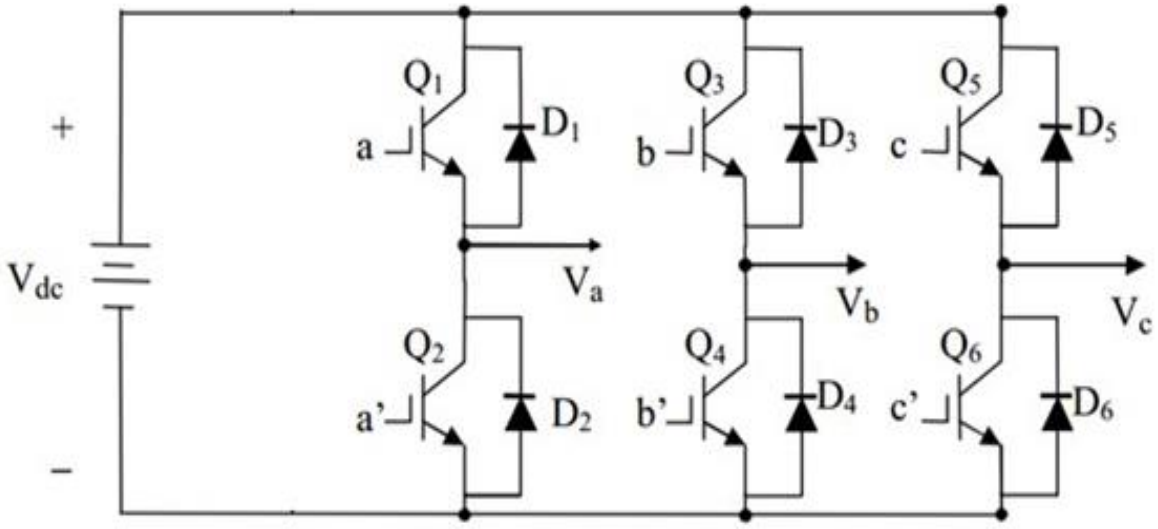

Figure 3.4 Three Phase Invertor [2]

The relationship between the switch variable vector $[a\ \ b\ \ c]^T$ and the line-to-line voltage vector $[V_{ab}\ V_{bc}\ \ V_{ca}\ ]^T$ of the Three Phase invertor [2] in Figure 3.4 by by is Given (3.14).

$$\begin{bmatrix} V_{ab} \\ V_{bc} \\ V_{ca} \end{bmatrix} = V_{dc} \begin{bmatrix} 1 & -1 & 0 \\ 0 & 1 & -1 \\ -1 & 0 & 1 \end{bmatrix} \begin{bmatrix} a \\ b \\ c \end{bmatrix} \quad (3.27)$$

Where [a b c] is a vector that represents The inverter's Upper Switches. Their on and off state determined based on the position of reference voltage and the two adjacent active vectors dwelling time. Also, a comparison of the switching variable vector $[a\ b\ c]^T$ and The expression for the phase voltage vector [V a V b V c]T is given below.

$$\begin{bmatrix} V_a \\ V_b \\ V_c \end{bmatrix} = \frac{V_{dc}}{3} \begin{bmatrix} 1 & -1 & 0 \\ 0 & 1 & -1 \\ -1 & 0 & 1 \end{bmatrix} \begin{bmatrix} a \\ b \\ c \end{bmatrix} \quad (3.28)$$

The upper power devices' on and off states are diametrically opposed to those of the lower power devices. As a result, after the states of the upper power transistors have been established, figuring out the states of the lower power transistors is straightforward. Table 3.1 displays the output line to neutral voltage (phase voltage) and output line-to-line voltages in terms of DC-link Vdc, as well as the three upper power switches' eight switching vectors.

Table 3.1 Switching Vectors, output line-to-line voltages, and output phase voltages

Voltage Vectors	Switching Vectors			Line to neutral Voltage			Line to line Voltage			$V\alpha$	$V\beta$
	a	*B*	*C*	*Van*	*Vbn*	*Vcn*	*Vab*	*Vbc*	*Vca*		
V0	0	0	0	0	0	0	0	0	0	0	0
V1	1	0	0	2/3	-1/3	-1/3	1	0	-1	2/3	0
V2	1	1	0	1/3	-1/3	-2/3	1	0	-1	1/3	$\frac{1}{\sqrt{3}}$
V3	0	1	0	-1/3	2/3	-1/3	-1	1	0	-1/3	$\frac{1}{\sqrt{3}}$
V4	0	1	1	-2/3	1/3	1/3	-1	0	1	-2/3	0
V5	0	0	1	-1/3	-1/3	2/3	0	-1	1	-1/3	$-\frac{1}{\sqrt{3}}$
V6	1	0	1	1/3	-2/3	1/3	1	-1	0	1/3	$-\frac{1}{\sqrt{3}}$
V7	1	1	1	0	0	0	0	0	0	0	0

(Remember to multiply the relevant Voltage by vdc.)

3.3.1 The space vector PWM principle

- Considers the Sinusoidal Voltage (*Vrf*) to be a vector with constant amplitude and constant rotational frequency. This PWM approach uses a mixture of the eight switching patterns to approximate the reference voltage Vref (*V0* to *V7*). Coordinate transition (from the stationary α-β frame to the a, b, and c reference frames).
- The plane is divided into six sectors by the vectors (*V1* to *V6*)(each sector,60 degrees).
- Two adjacent non-zero and zero-vector pair combinations result in *Vref*.

3.3.2 Space Vector PWM Implementation

The voltage equation in the a-b-c reference frame must be translated into the stationary *α-β* reference frame, which contains of the horizontal (α) and vertical (β) axes, in order to execute the space vector PWM. This results in the possibility of six non-zero vectors and two zero vectors. As shown in Figure 3.7, the axis of a hexagon is formed by six non-zero vecters, *V1* to *V6*, which can either supply the load with DC link voltage or electrical power. Using the eight switching patterns,To generate the average inverter output over a brief period of time with *Tz* equal to Vref over the same duration is one straightforward approximation method. Assume that the voltage phasor Vref has been ordered. As seen in Figure 3.5, it is positioned halfway between two switching voltage vectors, let's call them *V1* and *V2*, and it has a relative phase angle of from *V1*. Only by using the nearby switching voltage vectors, in this case *V1* and *V2*, can the requested voltage phasor be accomplished. Combining these switching vectors via the load produces the required command space voltage phasor because it is not possible to capture even a small portion of these switching vectors.

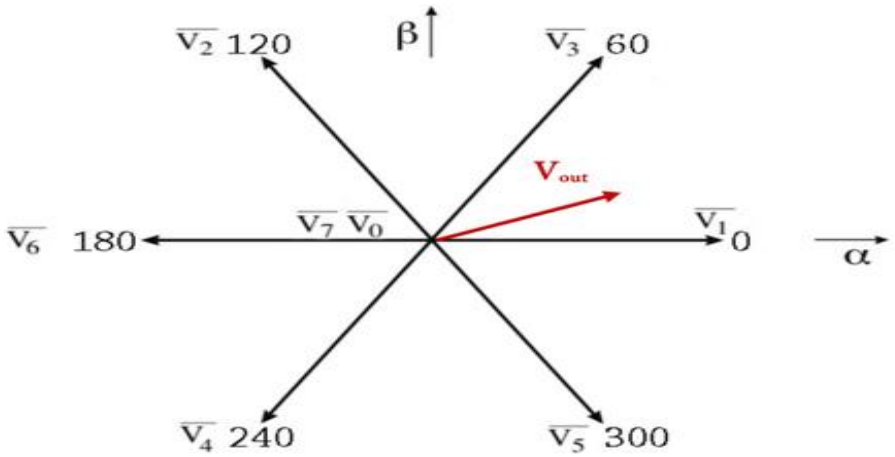

Figure 3.5 Sectors, fundamental switch vector,and a Reference Vector [2].

Therefore, The following procedures can be used to implement space vector PWM:

Step 1. CalculateVα,Vβ VRef,and angle alpha (α) to identify the particular sector.

Step 2.Calculate the time periods *T1, T2*, and T0 for the particular sector, where *T0* indicates the periods at which the null vectors *V0* and *V7* should be applied, and *T1, T2* represent the times at which the fundamental space vectors *V1* and *V2*should be applied, respectively, across the time range Tz.

Step 3. Identify each transistor's switching duration (*S1 to S6*).

Step 1: Calculate *Vα, Vβ, Vref,* and angle (α).

The *Vα, Vβ, Vref,* and angle (α) can be calculated using the coordinate conversion to 2-Φ Stationary reference frame shown in figure 3.6

$$V_\alpha = V_{an} - V_{bn}\cos(60) - V_{cn}\cos(60) = V_{an} - \frac{1}{2}V_{bn} - \frac{1}{2}V_{cn} \tag{3.29}$$

$$V_\beta = 0 - V_{bn}\cos(30) - V_{cn}\cos(30) = \frac{\sqrt{3}}{2}V_{bn} - \frac{\sqrt{3}}{2}V_{cn} \tag{3.30}$$

Therefore, The matrix form of the aforementioned equations is as follows.

$$\begin{bmatrix} \mathrm{V}_\alpha \\ \mathrm{V}_\beta \end{bmatrix} = \begin{bmatrix} 1 & -\frac{1}{2} & -\frac{1}{2} \\ 0 & \frac{\sqrt{3}}{2} & -\frac{\sqrt{3}}{2} \end{bmatrix} \begin{bmatrix} \mathrm{V}_{\mathrm{an}} \\ \mathrm{V}_{\mathrm{bn}} \\ \mathrm{V}_{\mathrm{cn}} \end{bmatrix} \tag{3.31}$$

The reference space vector voltage formula that spans each sector is

$$V_{ref} = \sqrt{{V^2}_\alpha + {V^2}_\beta} \tag{3.32}$$

The reference voltage vector's location in the current sector is defined by:

$$\alpha = \tan^{-1}\left(\frac{V_\beta}{V_\alpha}\right) = \omega t = 2\pi f t \tag{3.33}$$

Where f is the reference voltage's rotational frequency at its fundamental frequency.

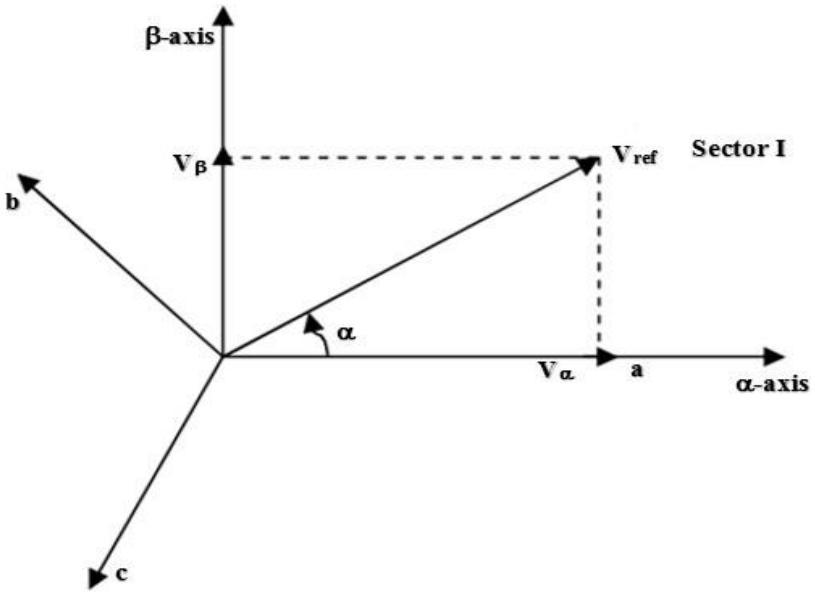

Figure 3.6 Voltage space vector and its elements along the a, b, and c axes[25]

Stap 2: Calculate the durations *T1, T2,* and *T0.*

Sector 1 switching time duration:

$$\int_0^{Tz} V_{ref}dt = \int_0^{T1} V_1 dt + \int_{T1}^{T1+T2} V_2 dt + \int_{T1+T2}^{Tz} V_0 dt \tag{3.34}$$

$$T_z V_{ref} = (T_1.V_1 + T_2.V_2) \tag{3.35}$$

The first sector's average voltage, which is comprised of the vectors *V0, V1, V2,* and *V7,* is given by (3.23).(Where, $0 \leq \alpha \leq 60$)

$$T_z|V_{ref}|.\begin{bmatrix}\cos(\alpha)\\ \sin(\alpha)\end{bmatrix} = T_1\frac{2}{3}V_{dc}\begin{bmatrix}1\\0\end{bmatrix} + T_2\frac{2}{3}V_{dc}\begin{bmatrix}\cos(\frac{\pi}{3})\\ \sin(\frac{\pi}{£})\end{bmatrix} \tag{3.36}$$

$$T_1 = T_z.a.\left(\frac{\sin\left(\frac{\pi}{3}-a\right)}{\sin\left(\frac{\pi}{3}\right)}\right) \tag{3.37}$$

$$T_1 = T_z.a.\left(\frac{\sin(\alpha)}{\sin\left(\frac{\pi}{3}\right)}\right) \tag{3.38}$$

$$T_0 = T_1 - (T_1 + T_2) \tag{3.37}$$

And

$$T_z = \frac{1}{fz} \; and \; a = \frac{|V_{ref}|}{\frac{3}{2}V_{dc}} \tag{3.38}$$

Where The switching times for vectors *V1* and *V2* are *T1* and *T2*, respectively. The zero vector's time duration is *T0*, while the application of one sector's time duration is *Tz*. The following equations provide switching time length for any sector:

$$\begin{aligned} T_n &= \frac{\sqrt{3}T_z |V_{ref}|}{V_{dc}} \left(\sin\left(\frac{\pi}{3} - \alpha + \frac{n-1}{3}\pi \right) \right) \\ &= \frac{\sqrt{3}T_z |V_{ref}|}{V_{dc}} .\sin(\frac{n}{3}\pi - \alpha) \\ &= \frac{\sqrt{3}T_z |V_{ref}|}{V_{dc}} .\sin\frac{n}{3}\pi.\cos\alpha - \cos\frac{n}{3}\pi.\sin\alpha) \end{aligned} \tag{3.39}$$

$$\begin{aligned} T_{n+1} &= \frac{\sqrt{3}T_z |V_{ref}|}{V_{dc}} \left(\sin\left(\alpha - \frac{n-1}{3}\pi \right) \right) \\ &= \frac{\sqrt{3}T_z |V_{ref}|}{V_{dc}} (-\cos\alpha.\sin(\frac{n-1}{3}\pi + \sin\alpha.\cos\frac{n-1}{3}\pi) \\ T_0 &= T_z - (T_n + T_{n+1}) \end{aligned} \tag{3.40}$$

Where *n* = 1 where 0 60 and n = 1 to 6 (sector 1 to 6) As shown in figure 3.7 for the first sector, the technique utilized to approach the target stator reference voltage with just eight different switch states is to combine consecutive reference voltage vectors and time the application of each neighboring vector.

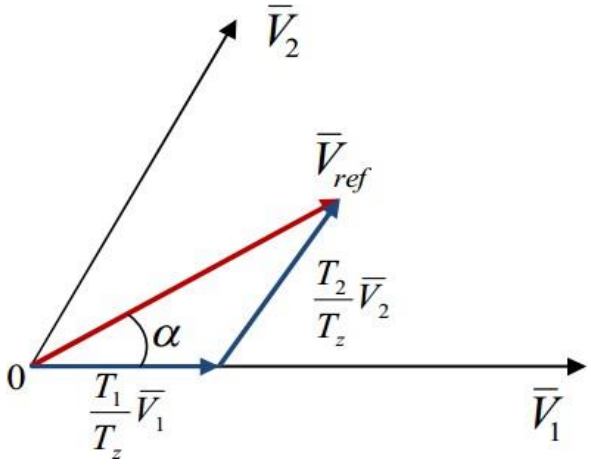

Figure 3.7 shows the reference voltage in sector I as a union of nearby vectors [25].

Step 3: Identify each transistor's switching duration (*S1* to *S6*).

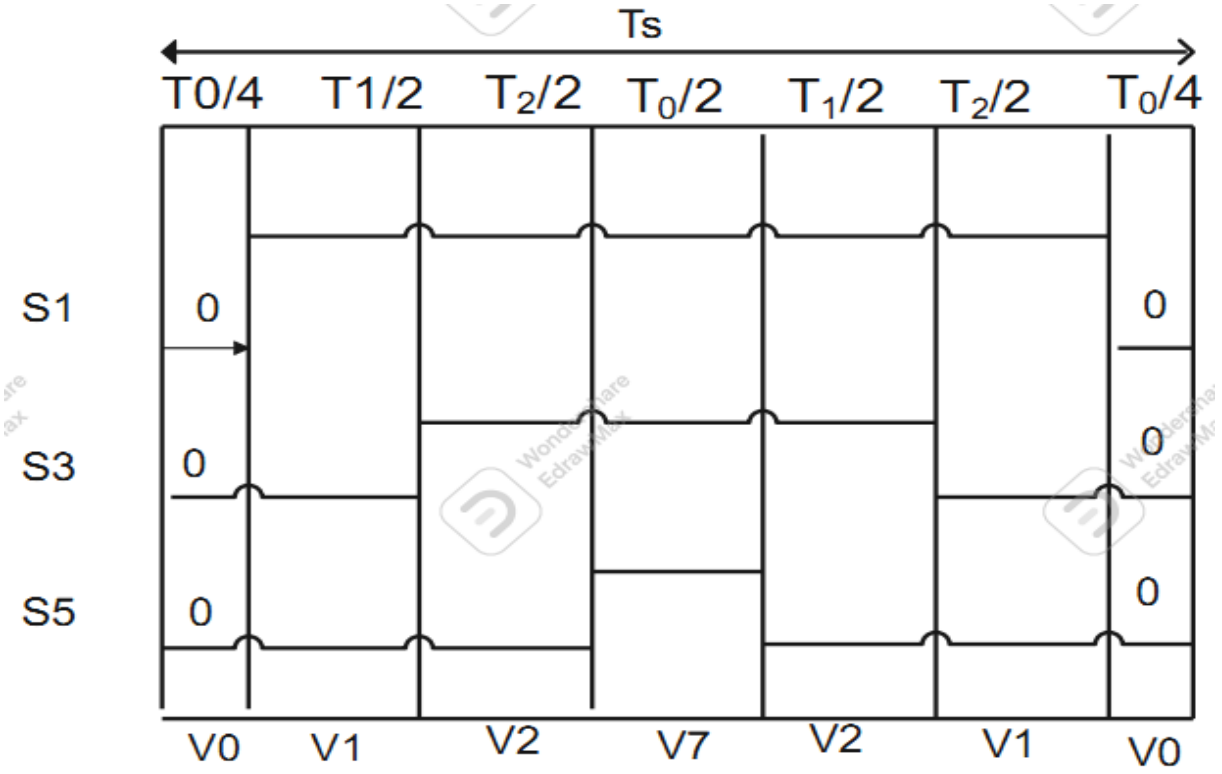

Figure 3.8 Switching configuration for the first sector of SVPWM[2]

The switching time in the first sector is compiled in table 3.2 based on Figure 3.8.

Table 3.2 Calculation of the first sector's switching time

Sector	Upper switch (*S1,S2,S3*)	Lower switch (*S2,S4,S6*)
1	$S_1 = T_1+T_2+T_0/2$	$S_2 = T_0/2$
	$S_3 = T_2+T_0/2$	$S_4 = T_0/2+T_1$
	$S_5 = T_0/2$	$S_6 = T_0/2+T_1+T_2$

The same formula used to compute the first sector's switching time can be applied to other sectors.

CHAPTER FOUR

4 CONTROLLER OF THE PMSM

4.1 Introduction

The FOC-based speed control of PMSM is composed of the internal Loop for Current and the outside Loop for Speed. The response time, or how rapidly they may be modified, determines the order of the loops. A Current Loop that is at least ten times quicker than the Speed Loop is necessary to prevent the time delay caused by the speed controller's cascaded control structure[2, 6].

4.2 PID controller design

With its minimal steady-state error, quick Response (short rise time), lack of Oscillations, and enhanced stability, the PID controller provides the best control dynamics. To prevent oscillations and overshoot in the system's output response, a derivative gain component must be used in adding to the PI controller.

Proportional (P): The main purpose of the P controller is to increase the system's responsiveness and decrease its steady state accuracy.

Integral (I) : It is primarily employed to get rid of steady state inaccuracy.

For ac machine drives, PI controllers are far more common than high frequency voltage source inverters (VSI), which cause chattering on the regulated signal and render derivative actions subject to measurement noise. As a result, a separate PI module with a transfer function of KP + Ki/s, where Kp is a proportional gain and Ki is an integral gain, controls all rotor speed, flux, and torque.

4.3 Current controller Design

The design of PID-controllers requires the closed loop transfer function. The following is the given d-q axis current open loop transfer function:

$$\frac{i_d}{v_d + w_r L i_q} = \frac{1}{L + R} \tag{4.1}$$

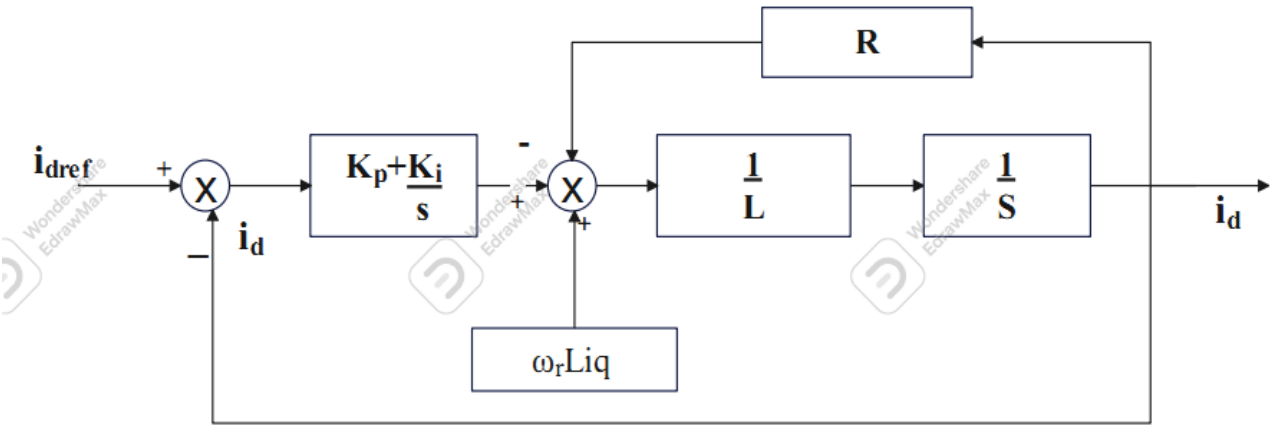

Figure 4.1 Block diagram for the d-axis

The q-axis current open loop transfer function from (3.6) can be, similarly to the d-axis current, as follows:

$$\frac{i_q}{v_q - w_r(Li_d + \lambda_m)} = \frac{1}{L+R} \tag{4.2}$$

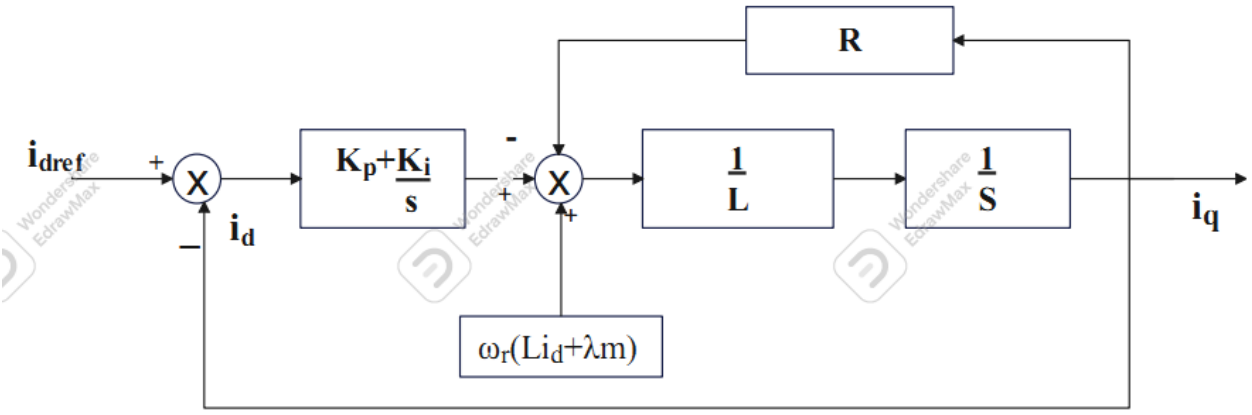

Figure 4.2 block diagram for the q-axis

According to Figures 4.1 and 4.2, the ωr Liq and ωr (Lid +m) blocks complicate the closed loop transfer function. The feed forward decoupling method ignores the ωr Liq and ωr (Lid +m) parts of the equation to simplify PI controller parameter calculation. The general transfer function between the reference's idref and the flux component's id is shown in Figure 4.1 as follows:

$$\frac{i_d(s)}{i_{dref}(s)} = \frac{K_p s + K_i}{Ls^2 + (K_p + R)s + K_i} \tag{4.3}$$

The entire Transfer function between the torque component iq and its reference, iqref, can be shown in Figure 4.2:

$$\frac{i_q(s)}{i_{qref}(s)} = \frac{K_p s + K_i}{Ls^2 + (K_p + R)s + K_i} \tag{4.4}$$

Because Ld= Lq=L for surface mounted PMSM, the closed loop transfer function of (4.3) and (4.4) are the same. As a result, the design of the q-axis current controller is sufficient to determine the d-axis current controller's controller parameter. By comparing the performance of the 2nd order closed loop system in (4.5) with (4.4) and (4.3), the current controller gain values of Kp and Ki in terms of motor parameters are found in (4.6) and (4.7).

$$\frac{\omega_n^2}{s^2 + 2\xi\omega_n s + \omega_n^2} \tag{4.5}$$

$$K_p = 2\xi\omega_n L - R \tag{4.6}$$

$$K_i = \omega_n^2 L \tag{4.7}$$

4.4 Speed Controller Design

The current controller ensures that the actual current follows the commanded current, whereas the speed controller ensures that the speed follows the commanded speed. The speed control system is modeled using the motor's electromechanical characteristics (4.8).

$$\frac{3}{2} p^2 \lambda_m i_{q(t)} = J \frac{dw_{r(t)}}{dt} + B w_{r(t)} + p T_{L(t)} \tag{4.8}$$

From equation (4.8) the speed differential equation determined as:

$$\frac{dw_{r(t)}}{dt} = \frac{3}{2}\frac{p^2 \lambda_m}{J} i_{q(t)} - \frac{Bwr(t)}{J} - \frac{p}{J} T_{L(t)} \tag{4.9}$$

Where, λm Magnetic flux, P number of pole pairs, J moment of inertia (kg/m2), B viscous friction coefficient of the motor (Nm s/rad) and wr electrical speed of the rotor. Applying the Laplace transformation to get the relationship between the angular velocity and the q- axis current.

$$\left(s+\frac{B}{J}\right)w_r(s)=\frac{3}{2}\frac{p^2\lambda_m}{J}i_q(s) \tag{4.10}$$

$$\frac{w_r(s)}{i_q(s)}=\frac{\frac{3}{2}\frac{p^2\lambda_m}{J}}{s+\frac{B}{J}} \tag{4.11}$$

Now from the current PI controller designing using performance specification the transfer function from the q-axis reference current to the actual q-axis current given by:

$$\frac{i_q(s)}{i_q(s)^*}=\frac{\left(2\xi\omega_n-\frac{R}{L}\right)s+\omega_n^2}{s^2+2\xi\omega_n s+\omega_n^2} \tag{4.12}$$

Substituting (4.11) transfer function in to (4.12), the relationship between the reference q-axis current $i_q(s)^*$ and the electrical speed wr(s) is given by:

$$\frac{w_r(s)}{i_q(s)^*}=\left(\frac{\frac{3}{2}\frac{p^2\lambda_m}{J}}{s+\frac{B}{J}}\right)\left(\frac{\left(2\xi\omega_n-\frac{R}{L}\right)s+\omega_n^2}{s^2+2\xi\omega_n+\omega_n^2}\right) \tag{4.13}$$

If the natural frequency ωn chosen to be much greater than the mechanical relationship B/J , the inner current-loop dynamics can be neglected, and the following first order model approximation can be taken as:

$$\frac{w_r(s)}{i_q(s)^*}\approx\frac{\frac{3}{2}\frac{p^2\lambda_m}{J}}{s+\frac{B}{J}} \tag{4.14}$$

From (4.14) it shows that the electrical speed controller output gives the reference quadrature current. Appling performance specification design technique like PI current controller using (4.5), the speed PI controller parameters can be calculated as follows.

$$K_p=\frac{2\xi\omega_n-\frac{B}{J}}{\frac{3}{2}\frac{p^2\lambda_m}{J}} \tag{4.15}$$

$$K_i = \frac{J\omega_n^2}{\frac{3}{2}p^2\lambda_m} \tag{4.16}$$

The outer-loop controller's band width is compared to the inner loop current controller system's band width. It is recommended that the bandwidth of the outer-loop system be between 5% and 10% of the bandwidth of the inner-loop control system [6, 29].

4.5 Model Predictive Controller Design

Predictive controllers are a type of controller that uses a system model to forecast the future behavior of the controlled variables. The controller uses this information to determine the optimal control input that minimizes a function-defined cost. It is possible to avoid the cascade structure, which is typically used in a linear control scheme by using this type of control. The system's nonlinearities can be incorporated into the model, eliminating the need to linearize it for an operating point. Some predictive schemes also allow for the consideration of actuator constraints and plant variables. Predictive control has several advantages that make it suitable for power converter control: its concepts are simple, it can be applied to a wide range of systems, and constraints and non-linearity are easily modelled. However, when compared to a traditional control scheme, they generally necessitate a large number of calculations.

Here is a copy of equation (3.17) from the previous section:

$$\begin{aligned} T_e &= \frac{3}{2}p[\psi_f i_q + (L_d - L_q)i_d i_q] \\ &= \frac{3p|\psi_s|}{4L_d L_q}[2\psi_f L_q \sin\delta + |\psi_s|(L_d - L_q)\sin 2\delta] \end{aligned} \tag{4.17}$$

Where p is number pole pairs, and fraction 3/2 stems from frame conversion: perpendicular stator $\alpha\beta$ into rotor dq.

The drive dynamics are as follows:

$$T_e - T_{load} = J\frac{dw_r}{dt} \tag{4.18}$$

Where T_{load} is the load torque and J is the kinematic chain's summary moment of inertia.

Based on (4.17) and (4.18) movement equation is:

$$\frac{dw_r}{dt} = \frac{p}{J}\left[\frac{3}{2}\left(\psi_f - \left(L_q - L_d\right)i_d\right)i_q\right] - \frac{T_{Load}}{J} \tag{4.19}$$

Rotor position γ can be described by the rotational speed derivative equation:

$$\frac{d\gamma}{dt} = p.w_r \tag{4.20}$$

True assumptions for this work are that load torque T_{load} is invariable in a narrow interval and is treated as a negligible external disturbance. The state space model is a classical discrete state-space model with sample time Ts:

$$\frac{d}{dt}T_{load} \approx 0 \tag{4.21}$$

$$\underline{x}_k = A_k\left(\underline{x}_{k-1}\right)\underline{x}_{k-1} + B_k\left(\underline{x}_{k-1}\right)\underline{u}_k \tag{4.22}$$

$$\underline{y}_k = C_k\left(\underline{x}_k\right)\underline{x}_k \tag{4.23}$$

The following state vector x was chosen for Unscented Kalman Filter synthesis:

$$\underline{x}_k = \left[i_d i_q \omega_r\ \theta\right]^T \tag{4.24}$$

So the system matrix A_k has a form:

$$A_k\left(\underline{x}_k\right) = \begin{bmatrix} 1 - T_s\frac{R}{L_d} & T_s.w_r\frac{L_q}{L_d} & 0 & 0 & 0 \\ -T_s.w_r\frac{L_d}{L_q} & 1 - T_s.\frac{R}{L_q} & -T_s.\frac{\psi_f}{L_q} & 0 & 0 \\ 0 & T_1 & 0 & 0 & -T_s.\frac{1}{j} \\ 0 & 0 & T_s & 1 & 0 \\ 0 & 0 & 0 & 0 & 1 \end{bmatrix} \tag{4.25}$$

Where

$$T_1 = \frac{3}{2}p[\psi_f i_q + (L_d - L_q)i_d i_q]$$

The C_k is the rotating matrix Clark/Parck transformation:

$$C_k\left(\underline{x}_k\right) = \begin{bmatrix} \cos\theta & -\sin\theta & 0 & 0 \\ \sin\theta & \cos\theta & 0 & 0 \end{bmatrix} \tag{4.26}$$

And matrix $B_{k:}$:

$$B_k\left(\underline{x}_k\right) = \begin{bmatrix} T_s.\frac{1}{L_d}\cos\theta & T_s.\frac{1}{L_d}\sin\theta \\ -T_s.\frac{1}{L_d}\sin\theta & T_s.\frac{1}{L_d}\cos\theta \\ 0 & 0 \\ 0 & 0 \\ 0 & 0 \end{bmatrix} \tag{4.27}$$

$$\underline{x}_{MPC} = \left[i_d i_q \omega_r\ \theta\right] \tag{4.28}$$

State matrices would be simplified in turn. Torque at load T_{load} is considered a known disturbance. The method of control is determined by the appearance of the model of decoupled dq axes. Let the linear discrete-time state space equations describe the model of the plant to be predicted and controlled.

$$\begin{aligned} \underline{x}_{k+1} &= A\underline{x}_k + B\underline{u}_k \\ \underline{y}_k &= C\underline{x}_k + D\underline{u}_k \end{aligned} \tag{4.29}$$

$\underline{x} \in X \in \mathbb{R}^n$, $\underline{y} \in Y \in \mathbb{R}^p$, $\underline{u} \in U \in \mathbb{R}^m$ are state, output, and input vectors, respectively. In general, the cost function J_N that must be minimized in the receding horizon N has the quadratic form:

$$J_N = \sum_{j=k}^{k+N-1} \left(\underline{x}_j^T Q \underline{x}_j + \underline{u}_j^T R \underline{u}_j\right) \tag{4.30}$$

When we assume N step prediction, we can determine system output behavior in N subsequent steps such as:

$$y = O_N \underline{x}_0 + H_N \underline{u}_0 \tag{4.31}$$

Where

$$H_0 = D,\ H_k = CA^{k-1}B,\ k = 1, 2, \cdots, N-1$$
$$O_0 = C,\ H_k = CA^{k-1},\ k = 1, 2, \cdots, N-1$$

Based on the preceding and the definition of optimization cost in equation (4.30), they can be compared to the desired state of the system:

$$J_N = \sum_{p=0}^{N-1} \left(\underline{w}_p - \underline{y}_p \right)^T \left(\underline{w}_p - \underline{y}_p \right) = \left[\left(w - y \right)^T \left(w - y \right) \right]_N \tag{4.32}$$

Because it provides control, the optimizer should be an important part of the strategy. The quadratic programming (QP) problem can be solved by combining (4.30) and (4.32).

$$J_N = U^T H_N^T H_N u + 2\left(x_0^T O_N H_N - w^T H_N \right) \tag{4.33}$$

In order to minimize the value of the control signal ***u*** in each future predict state N The reference speed signal was fed into the w vector. Because the problem is dependent on the current state x, MPC requires the on-line solution of a QP at each time step *k*. Based on determining the analytical value min of the defined cost function (4.33), the following form is obtained:

$$\min J_N \rightarrow \min_u \frac{1}{2} u^T H u + fu \tag{4.34}$$

It is possible to impose some constraints that follow the rule:

$$Au \le b \tag{4.35}$$

In terms of maximum feed voltage:

$$\underline{u}_{\min} \le \underline{u}_k \le \underline{u}_{\max} \tag{4.36}$$

And the predicted state constraints:

$$\underline{x}_{\min} \le \underline{x}_k \le \underline{x}_{\max} \tag{4.37}$$

In this consideration, special attention was paid to the dq axis current (*id* and *iq*) limitation and the maximum supply voltage (v_α and v_β). Other restrictions appear to be unnecessary in that application. Author [24] presents a review of the state of the art in predictive control in power electronics and motor controllers. The iq and id components are proportional to torque and flux, respectively. The FOC strategy recommends *id* = 0, which is equivalent to recommending a control strategy that maximizes torque per ampere of stator current. The machine control is thus implemented as a current control, with the current commands generated by the external speed control loop. I assume in this thesis that the torque/current set points (speed control outputs) are known. The machine model is used to predict the future behavior of currents. Using Euler's approximation for the derivatives at a sampling time Ts,

$$\frac{di}{dt} \approx \frac{i(k+1)-i(k)}{T_s} \tag{4.38}$$

The equations of the predicted currents are deduced in the reference frame dq, where the superscript p indicates that it is a predicted value.

$$\begin{aligned} i_d^p(k+1) &= (1-\frac{RT_s}{L}).i_d(k) + T_s.\psi_f.i_q(k) + \frac{T_s}{L}.u_d(k) \\ i_q^p(k+1) &= (1-\frac{RT_s}{L}).i_q(k) + T_s.\psi_f.i_d(k) - \frac{T_s}{L}.K_t\psi_f + \frac{T_s}{L}.u_d(k) \end{aligned} \tag{4.39}$$

The equations in (4.39) allow for the prediction of current values based on the control inputs ud and uq. The issue then is determining the best voltage values to direct current to the desired reference. Model predictive control (MPC) is a type of control in which the current control action is derived from the online resolution of an optimal control problem over a given time horizon. Each sampling period is finite. The current state of the plant is used as the starting point for this. The optimization process generates a series of control actions that minimize a cost function. The plant only receives the first control action, and the process is repeated in the following sampling period. The MPC is a method that allows for the consideration of plant constraints as well as actual actuators. It is particularly useful in process industries with plants whose dynamics are relatively slow, allowing for real-time implementation [22]. The MPC is a type of control algorithm that uses:

- A model of the internal dynamics of the process.
- A cost functions over the forecast horizon. This function can take into account the values of the outputs and/or the inputs. It is calculated at each sampling instant k, given an initial state of the plant x (k). The goal is to minimize this function over a finite horizon of time N.
- An optimization algorithm that minimizes the cost function using the control input. This generates the optimal control sequence from time k.

Although the optimizer generates a sequence of inputs along the prediction horizon, in general only the first element is used. In the next sampling period, the new system state $x(k+1)$ is measured and another optimization is performed. Then, when designing a predictive model controller, one must take into account the sampling interval Ts, an appropriate cost function, and the forecast horizon N. In general, the forecast horizons long generate better performance.

However, the optimization problem must be computed online to find the optimal controller output for each sampling instant. The model of the plant is the one deduced in (4.39). These equations establish the relationship betweena control input and the predicted response at the next instant. In every moment of sampling k, given a state of the plant x(k), the state of the plant must be calculated in the next sampling instant, from an input vector u(k), to be optimizedto minimize the cost function. The choice of this function is directly related for the purpose of control. For the application of this work, the following function is used,which minimizes the error between the current setpoint and the prediction at the next instant ofsampling [23].

$$g = \left[i_d^*(k) - i_d^p(k+1) \right]^2 + \left[i_q^*(k) - i_q^p(k+1) \right]^2 \tag{4.40}$$

The optimization algorithm is presented as a search problem, in which there must be try different values of stress udq and choose those that minimize the given function from of the predicted value of the current. Given the discrete nature of power converters, it is possible to solve the MPC problem without the use of modulators by taking into account the discrete states of the electronic switches. Then, the problem is reduced to the evaluation of all possible states and the selection of the one that minimizes the cost function. This technique is called a predictive control model with a finite set of control states (Finite Control Set Model Predictive Control, FCS-MPC) [26]. Figure 4.3 shows a diagram of this method.

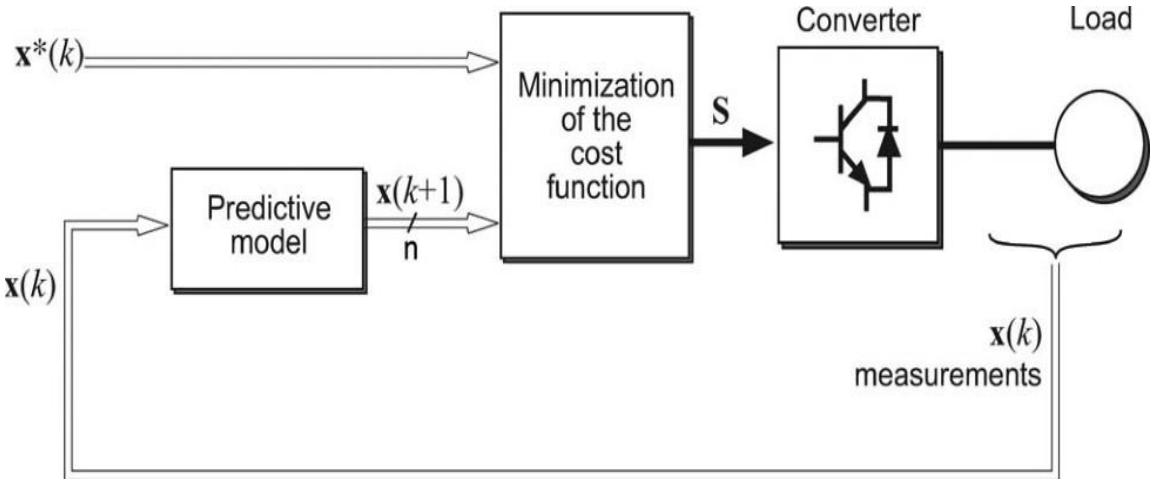

Figure 4.3 Diagram of the FCS-MPC

- Measure the stator currents x(k).
- Predict the current for the next sampling instant x(k+1) for all 8 of the possible states of the converter (6 active and 2 null).

- Evaluate the cost function for each prediction.
- Select the state that minimizes the cost function and apply it to the motor for a period full sampling. Figure 4.4, in which x represents the state variable of active system and U the input to be chosen, provides a clear illustration of this concept.

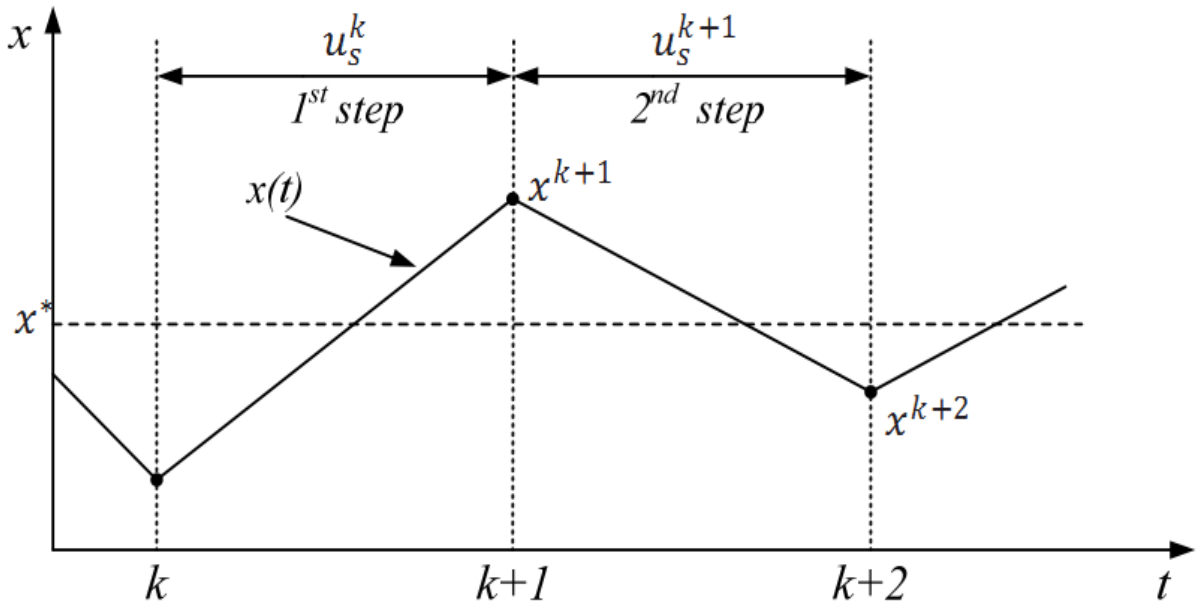

Figure 4.4 One-step delay in digital control systems.

CHAPTER FIVE

5 RESULTS OF THE SIMULATION AND DISCUSSION

5.1 Introduction

The simulation results of closed loop speed control of PMSM using model predictive control system with Matlab/Simulink are discussed in this chapter of the thesis. Only the operation of the PMSM below the base speed is shown in the simulation results will be explained.

5.2 Model of PMSM Drive System in Simulink.

Figure 5.1 illustrates The overall PMSM drive and control system Matlab/Simulink model. To investigate the simulation result, all of the components of the real drive system are modelled.

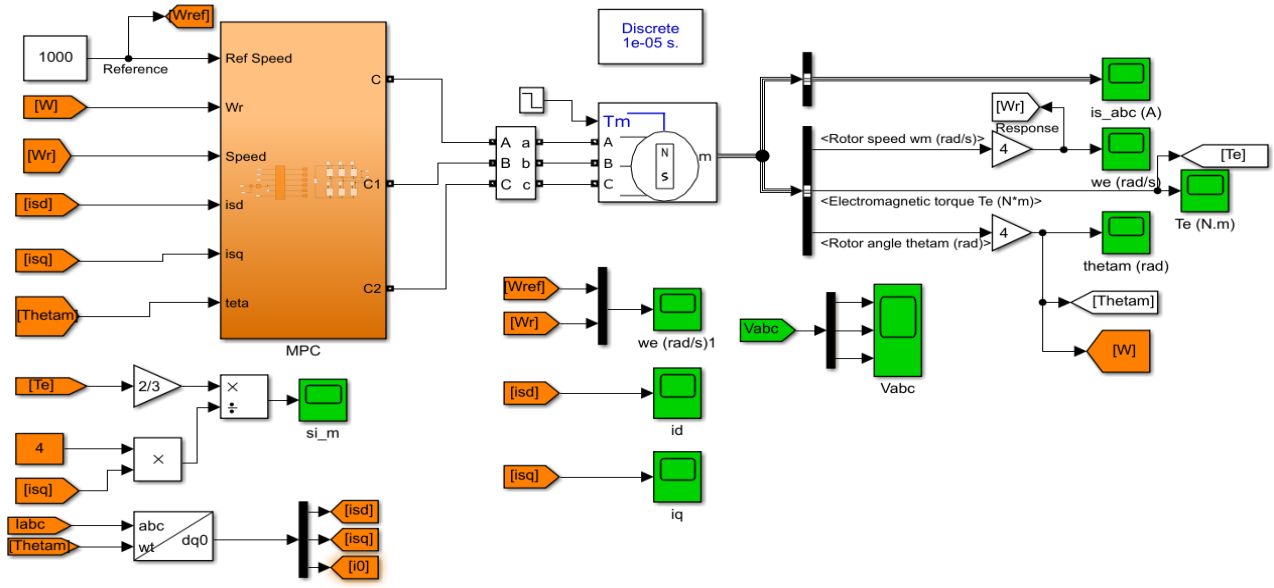

Figure 5.1 PMSM Drive complete Matlab/Simulink model.

The voltage vector for the PMSM is chosen using the cost function. After minimizing the cost function, the voltage vectors will be applied to the inverter so that the phase currents of the PMSM reach the expected current references in the next sampling time. As a result, the predictive current will be applied to the motor and it will operate in accordance with the references. The cost function for current PMSM prediction is given as equation (4.39). Assuming that the initial value of the cost function is infinite, the states of the MOSFETs will be determined when the temporary variable j changes from 0 to 7. The predicted current in the *d-q* axis can then be calculated using equations (4.39) and (4.40). Finally, if the temporary

variable j = 7, the states of the MOSFETs will be obtained using the cost function given in equation (4.40). Appendix B contains the corresponding control algorithm code.

5.3 Simulation Results

The PMSM drive's general Matlab/Simulink model and the MPC for PMSM speed control approach both allow for the simulation of machine behavior in a number of operating modes.

5.3.1 Speed Control Simulation Result

To evaluate the performance of the PMSM motor drive, the simulation result of MPC-based speed control was performed. Knowledge of the motor's parameters is important for this simulation because the estimator is highly parameter dependent, and the effect of parameter variation was tested based on different conditions and their effects on the robustness of the speed control. The comprehensive Matlab/Simulink model of the PMSM drive enables simulation of machine behavior for various operating modes using sensored feedback and MPC. First, the system's response to step speed input is tested, followed by the speed response to successive step levels. Second, for torque variation, the impact of machine speed response is simulated.

The speed response is then simulated and compared to the PI Controller's speed response to determine how the friction coefficient and moment of inertia parameter changes affect it.

Figure 5.2 illustrates the motor's speed response when commanded at a reference speed of 1500rpm.

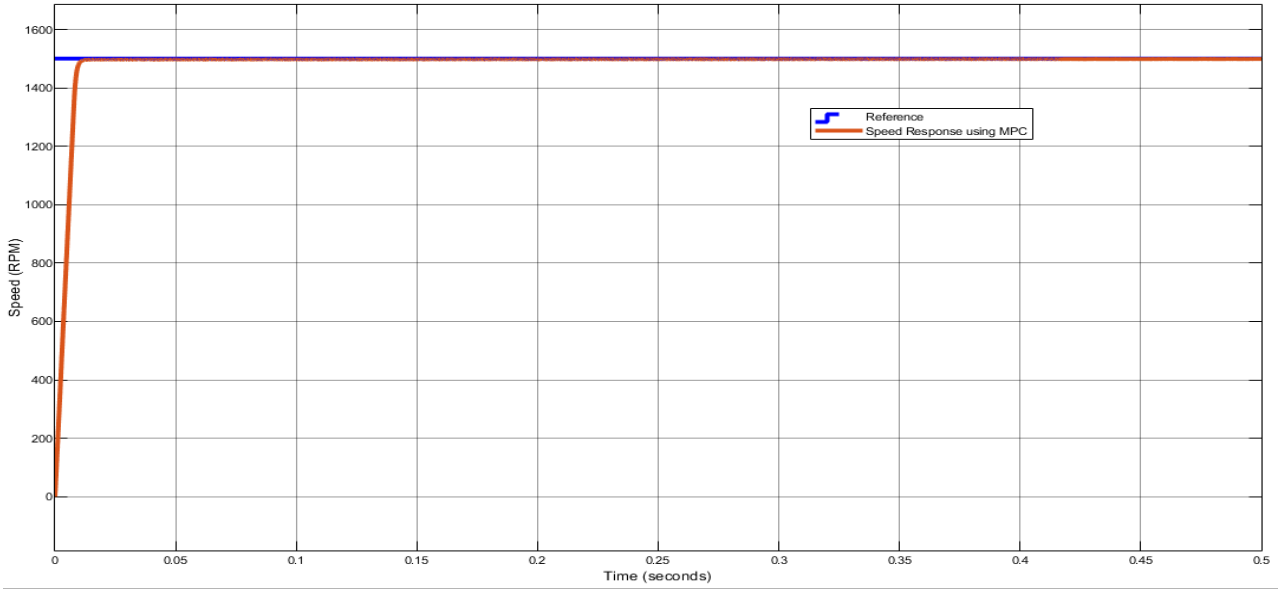

Figure 5.2 Machine speed response at a reference speed of 1500 rpm.

The developed electromagnetic torque is illustrated in Figure 5.3. The starting torque is around 57.32Nm until 0.0sec, which is primarily due to the rotor accelerating to a steady speed of 1500 rpm. When compared to the steady state value the starting torque is greater.As a result,the generated toque is intended to support rotor acceleration and friction delay Without the load torque (TL=0). However,after 0.01sec,the created toque is almost 0Nm, tolerating only the about zero delay friction to be supported.

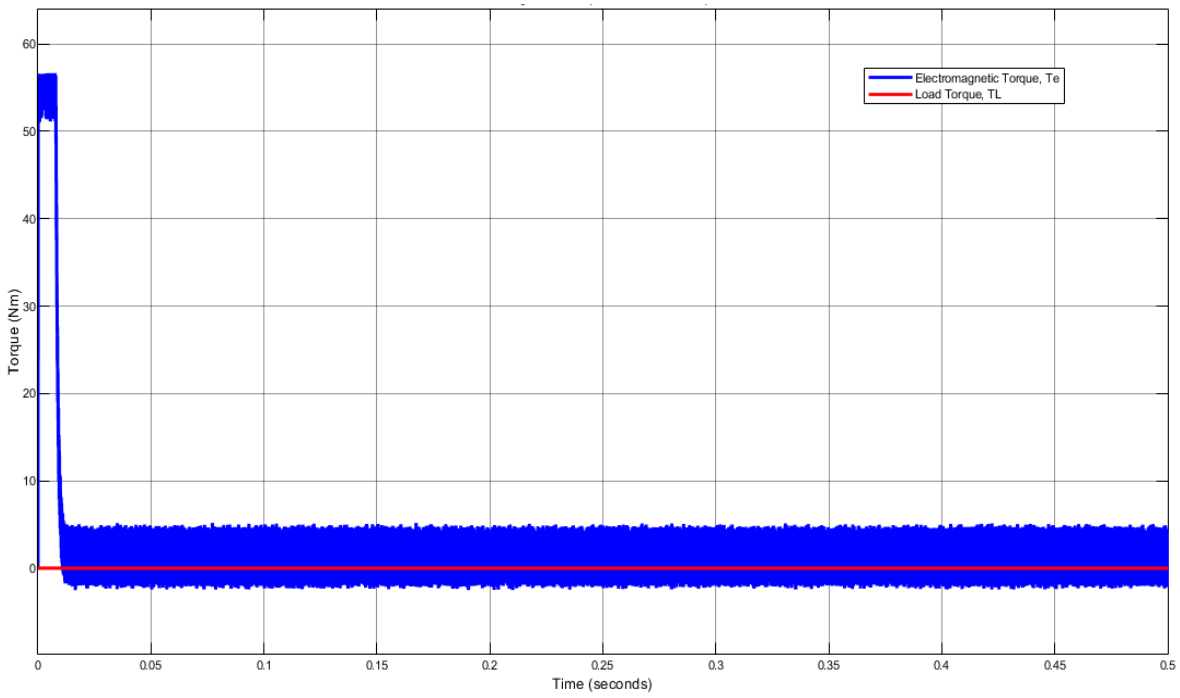

Figure 5.3 Step speed input's electromagnetic torque was developed.

When the motor is running at steady state and the controller command speed, the current is obviously non-sinusoidal at first and changes to sinusoidal. The motor's three phase currents (ia, ib, and ic) when it is operating at a constant speed are displayed in Figure 5.4.

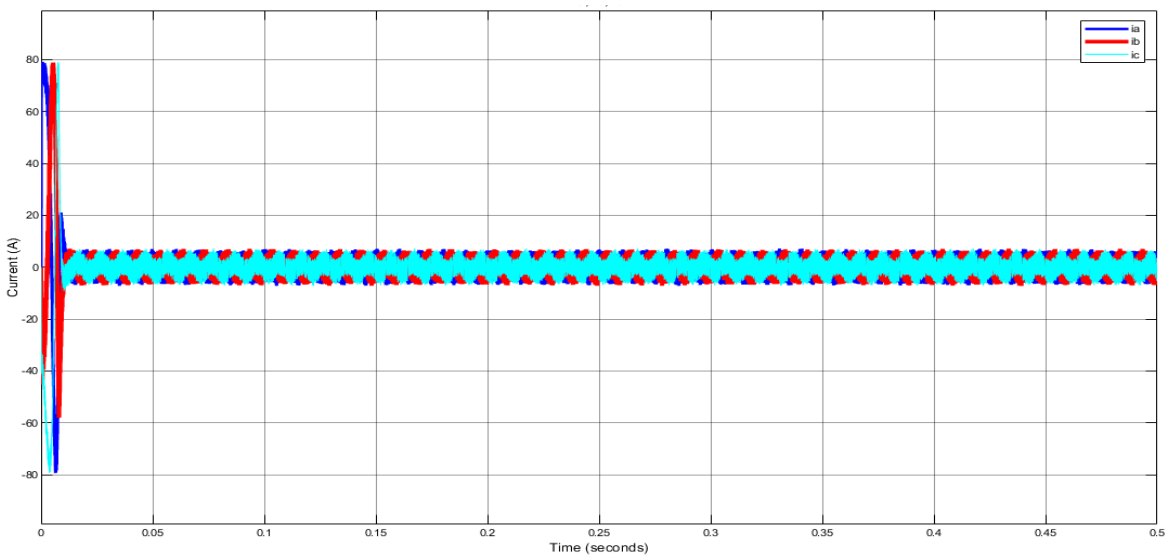

Figure 5.4 ia, ib and ic current as motor accelerating to 1500rpm speedinput.

Figure 5.5 illustrates the motor's speed response for a 1500rpm reference speed input to the PI controller and MPC.

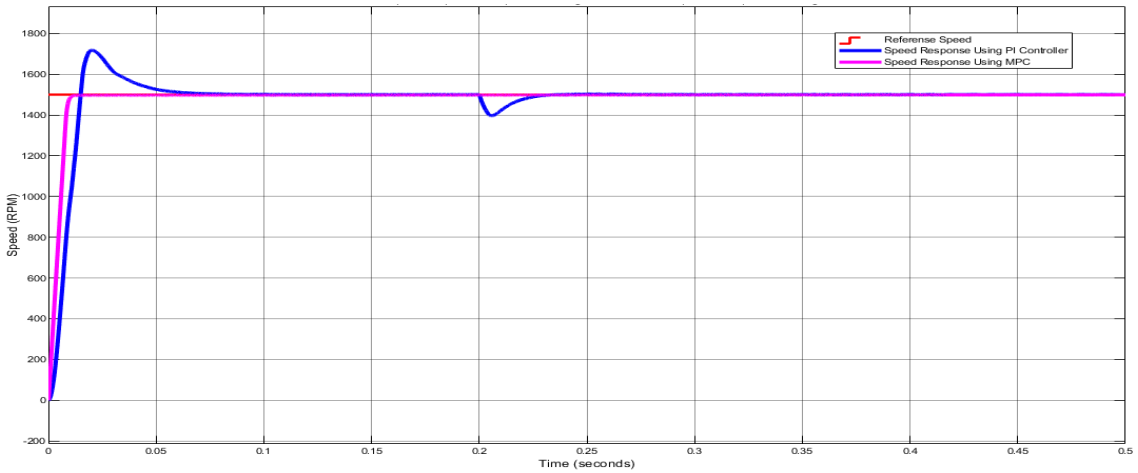

Figure 5.5 Response of PI and MPC Controllers in terms of speed with a reference speed input of 1500 rpm.

The machine's speed response for two ramping step speed level wants is shown in Figure 5.6. The target speed is initially set at 500rpm.At t = 0.019s, the speed abruptly shifts, reaching a constant 1500rpm. Figure 5.7 shows the machine's response to two ramping step speed level orders in terms of speed, while Figure 5.8 shows the machine's response in terms of current drawn.

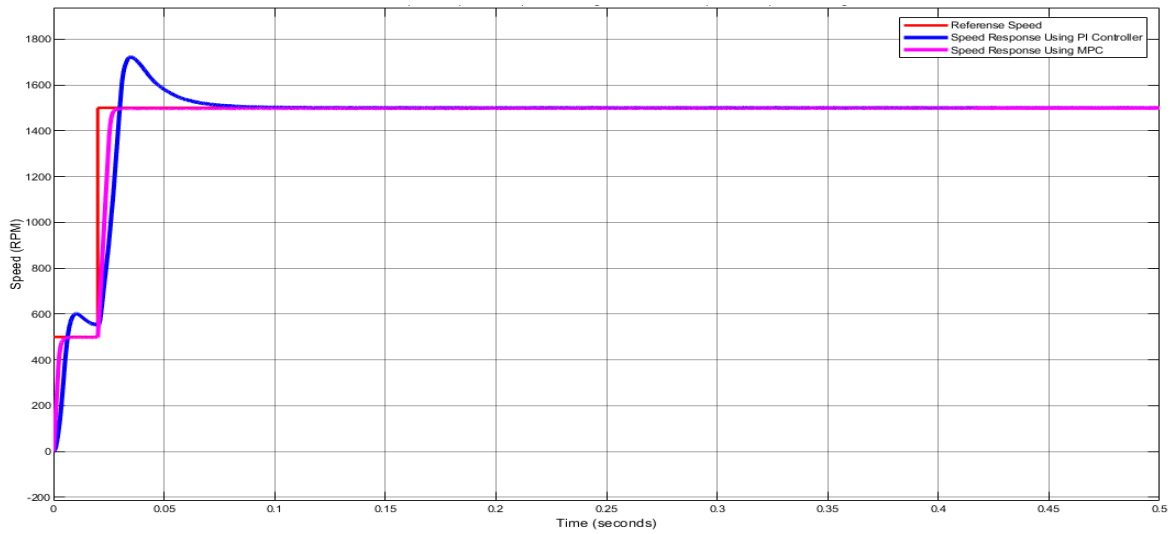

Figure 5.6 At two ramping step speed levels, reference speed and speed response are provided.

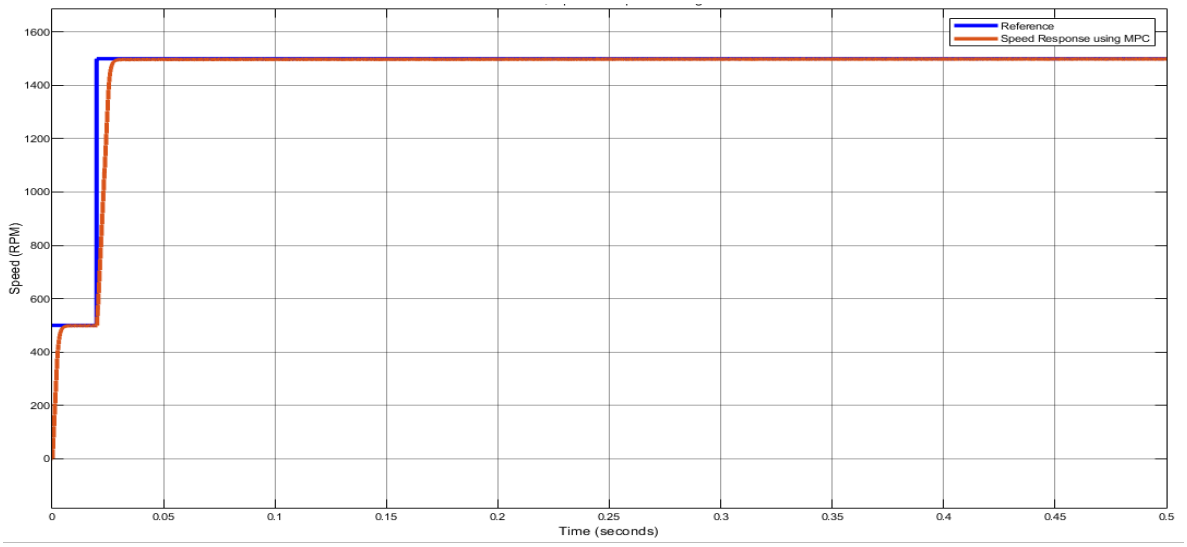

Figure 5.7 Reference speed and response for the MPC's two ramp speed levels.

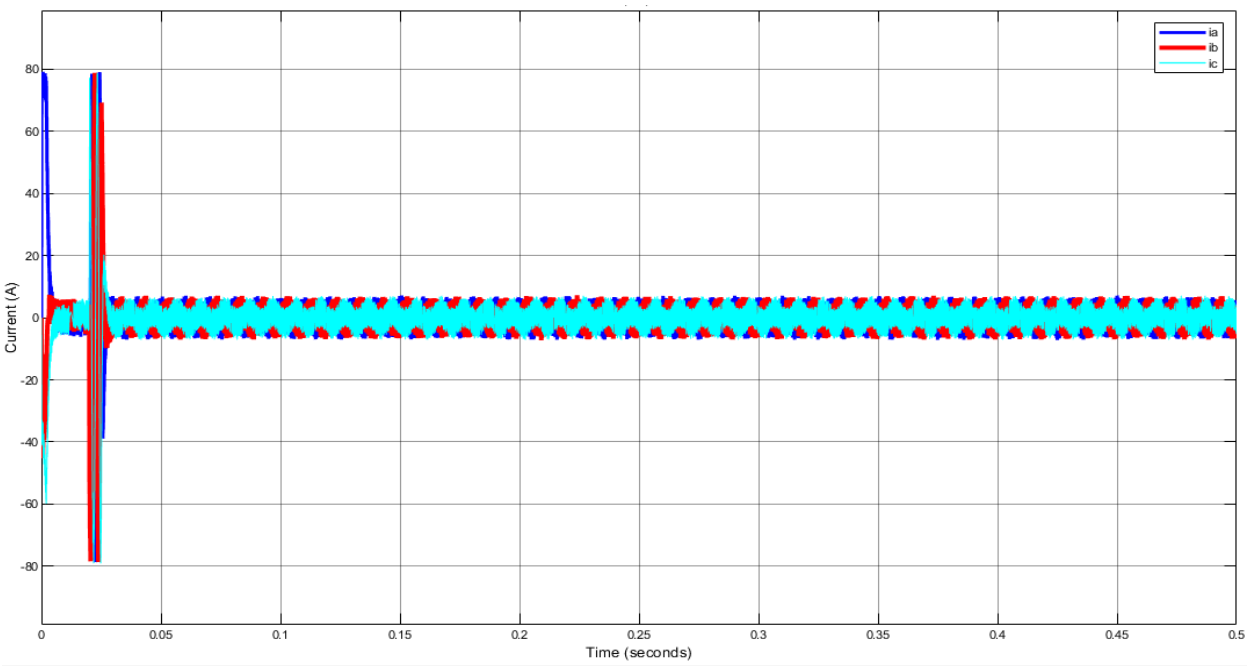

Figure 5.8 Motor current used for MPC's two level speed directives.

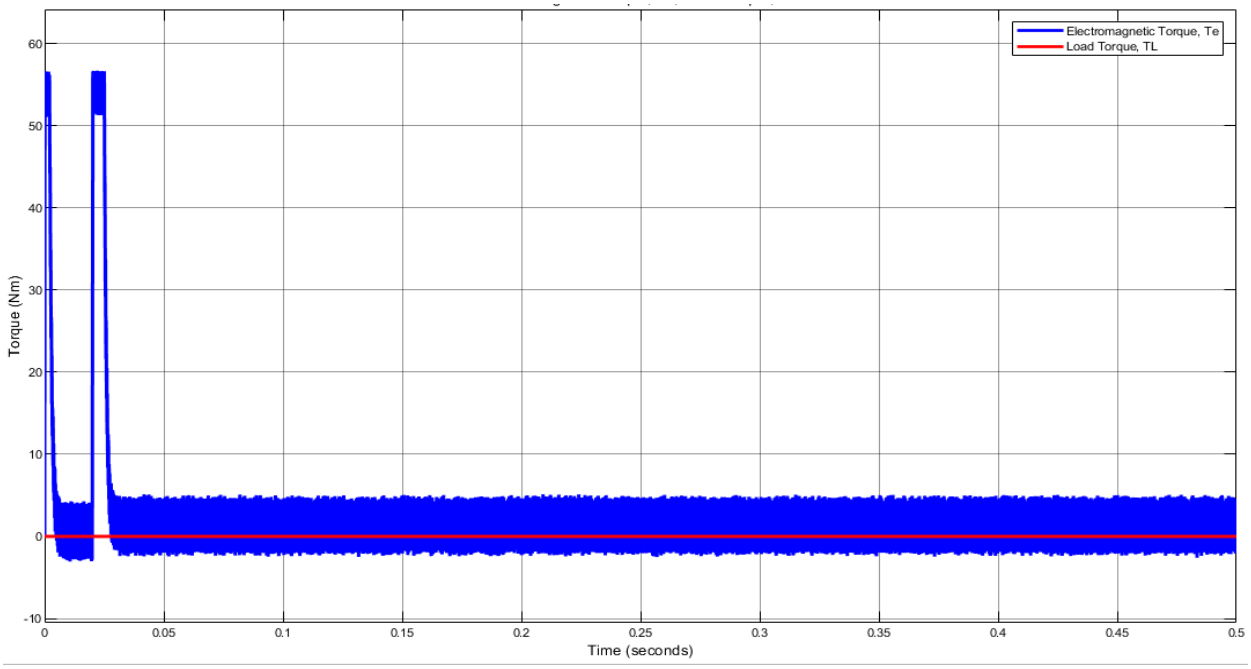

Figure 5.9 Magnetic torque produced for the MPC's two-step level speed input.

Figures 5.10 and 5.11 illustrate the Speed Response of the structure when the motor instant of inertia is 50% greater than nominal and when the motor friction coefficient is 50% greater than nominal without load torque, respectively. The controller's performance degrades to some amount, as evidenced by rising peak overshoot, rising settling time, and falling rise time, as shown in Figures 5.10 and 5.11.

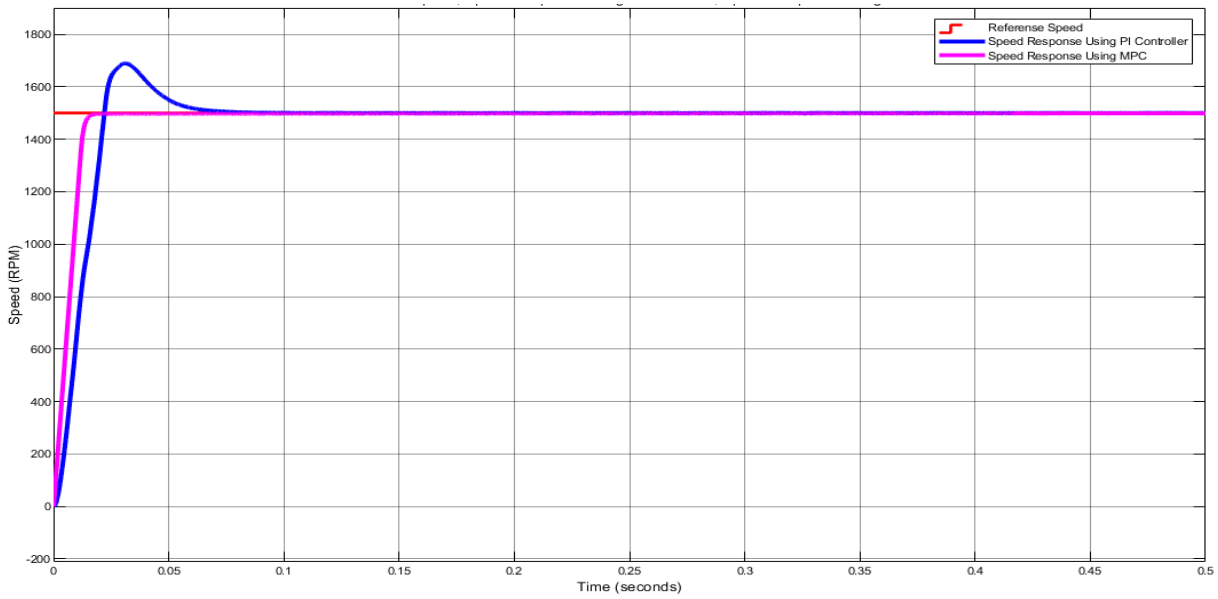

Figure 5.10 Moment of inertia response speed when increased by 50%

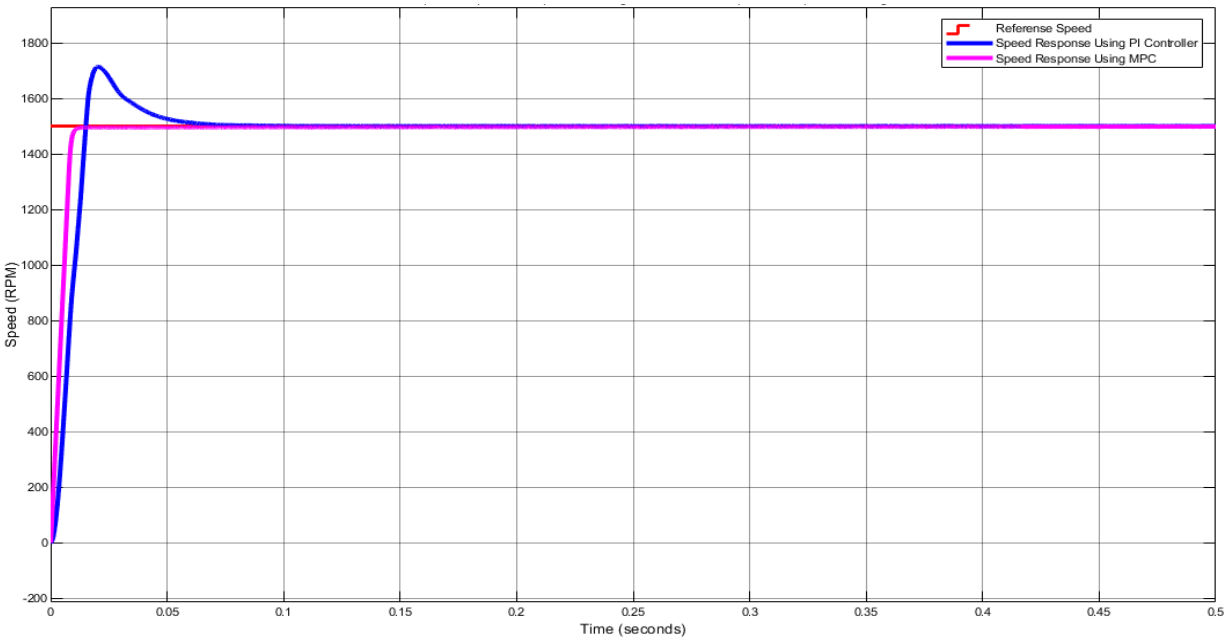

Figure 5.11 Speed reaction at a 50% increase in friction coefficient.

The system's speed and torque response to changes in load torque are shown in Figures 5.12 and 5.13. The drive system is initially started with zero load torque, then a continuous load of 10N.m is applied at t=0.007sec, followed by another zero load torque application at t=0.007sec, then a step load torque application of -10N.m at t=0.28sec. Figure 5.12 displays the machine's speed reaction to changes in load torque applied by the MPC and PI controller.As seen in the figure, at t=0.007sec, the speed would decrease when a positive external load torque was

applied, and at t=0.198sec, the opposite would occur. It demonstrates that PI controllers are unable to quickly recover from external load disturbances. The torque generation for the load torque application is shown in Figure 5.13. The current used by the motor as a result of the load disturbance described earlier is shown in Figure 5.14.

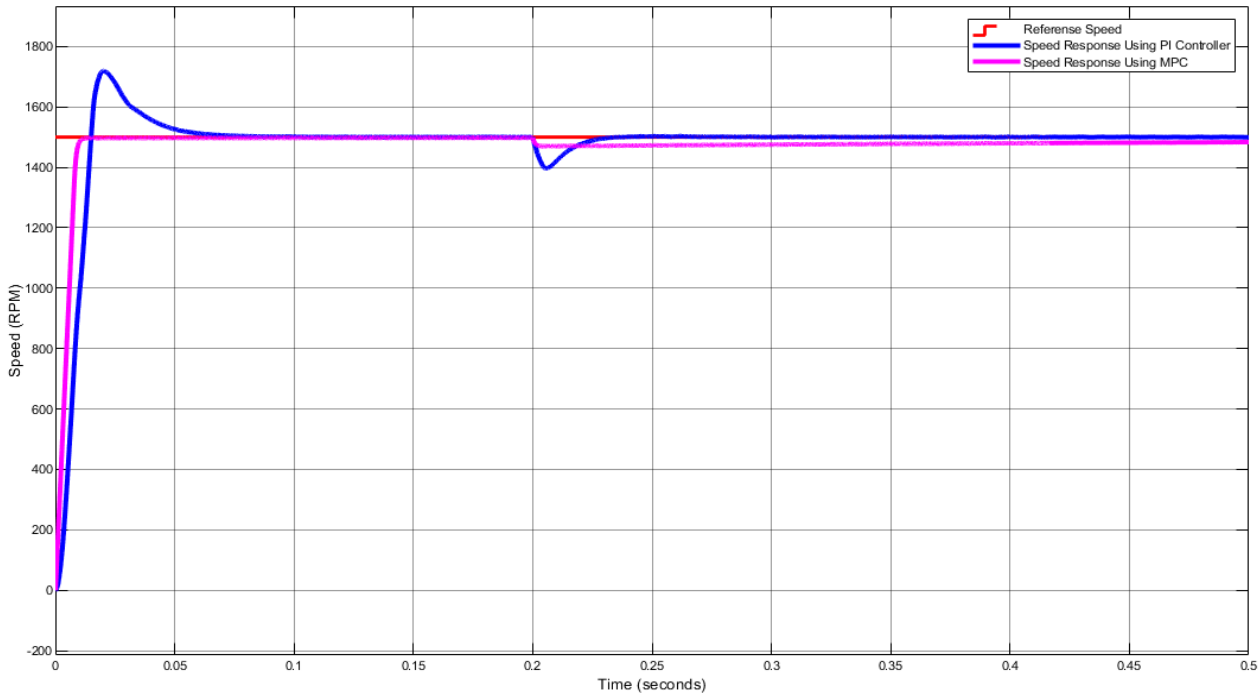

Figure 5.12 Response of speed to load torque variation.

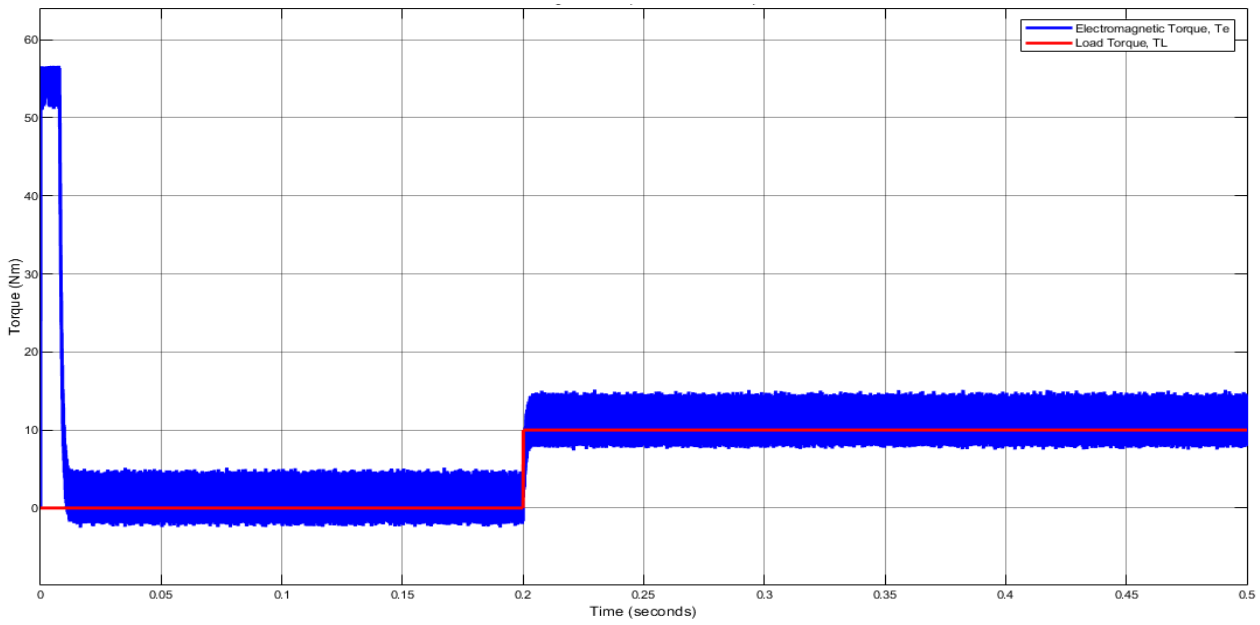

Figure 5.13 The torque produced by the load and the electromagnetic torque.

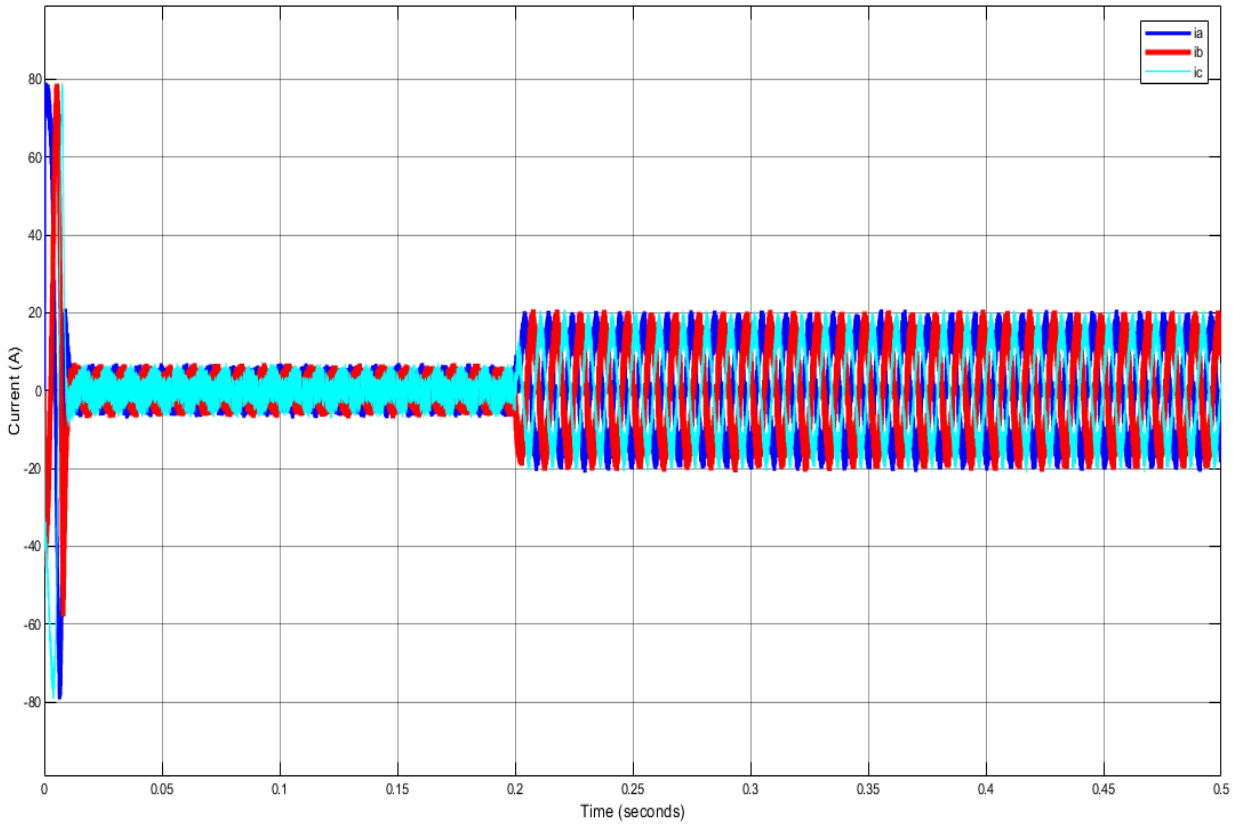

Figure 5.14 The machine's three-phase currents when the load torque changes.

5.3.2 Evaluation of the Performance and Stability of the MPC and PI Controller

a. Stability and performance assessment based on reaction

The stability and effectiveness of MPC are assessed using the system's response curve.The system's responsiveness to changes in its inputs is shown by the response curve. We look into a select group of common signals, including unit step and unit ramp. A system is deemed effective by a control engineer if it reacts well to these signals.

b. Performance and stability indicators

The system responses from the aforementioned simulation results as well as its parameters, such as overshoot, rising time, settling time, and steady state error, are used to assess stability and performance. The results of the simulation demonstrate that the MPC has a shorter regulating time and a speedier recovery from speed fluctuations and load disruptions. The outcomes demonstrate the stability of the developed MPC controller.

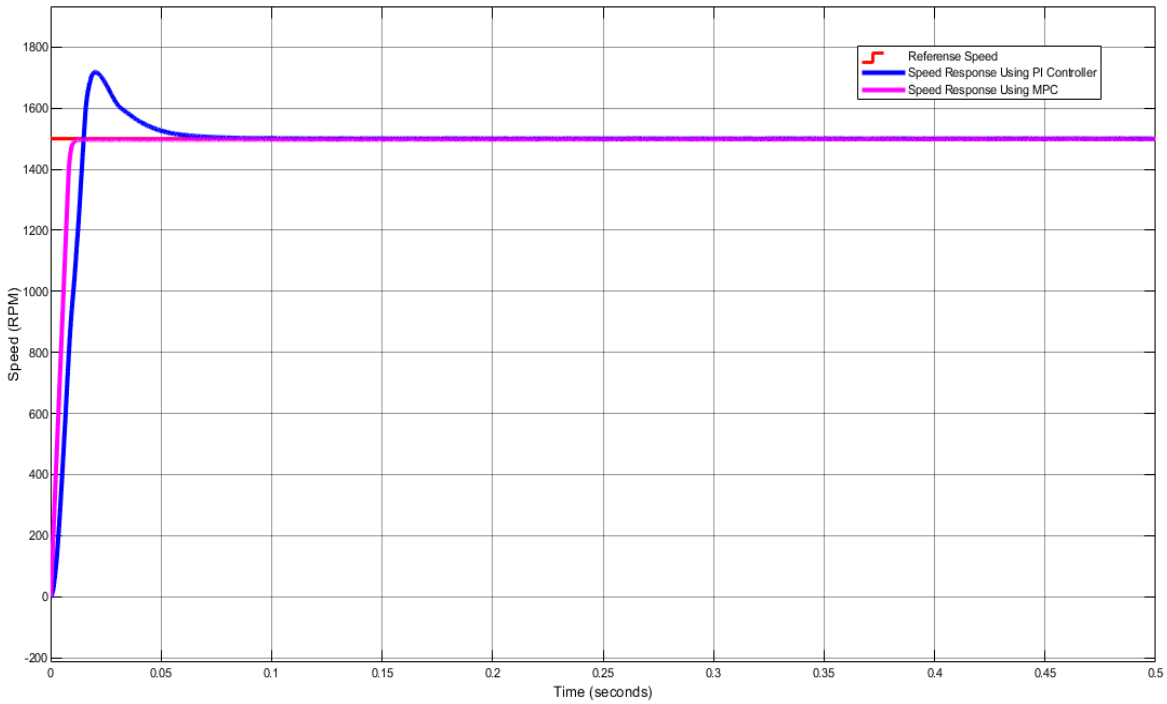

Figure 5.15 The MPC Performance parameters

Table 5.1 MPC and PI Controller Performance Comparison

No	Performance Indices	PI	MPC
1	1500 rpm overshoot with no load applied to the torque	14.368%	1.482%
2	Settling time(t_s) at 1500rpm, no load torque applied	-	4.5msec
3	Rise time at 1500rpm, nolead torque applied	10.608msec	6.102msec
4	Response speed	1709rpm	1497rpm
5	Overshoot at 1500rpm, 10 N.m Load torque applied	14.368%	0.490%
6	Settling time at 1500rpm, 10N.m Load torque applied	-	4.5msec
7	Rise time at 1500rpm, 10Nm load torque applied	10.608msec	6.102msec
8	Response speed	1380rpm	1478rpm

CHAPTER SIX

6 CONCLUSION AND RECOMMENDATION

6.1 Conclusions

The thesis provided a comprehensive investigation of permanent magnet synchronous machines.

The PMSM system is a challenging, time-varying, nonlinear system. Under conditions requiring a higher degree of accuracy, traditional PI controller results such as PMSM speed control fall short of expectations. In the PMSM control system, the controller serves as the speed control. Based on the speed error and the rate at which it changes, the controller can instantly modify the PI controller's parameters. The Matlab/Simulink software suite was used to simulate the entire system. The controller, inverter, and machine are all included in the simulation of the full system. The three modes of operation that are evaluated are the behavior with variable load torque at constant speed, the performance with variable speed for variable load torque, and the speed response for variable friction coefficient and moment of inertia. The simulation results demonstrate that MPC performs better than the conventional PI controller with constant gains in terms of a fast recovery from load changes and parameter changes, a short settling time, and a reduced overshoot. Than the MPC is contrasted with a PI controller. The control performances of the MPC demonstrate its effectiveness: the overshoot, settling time, and stationary regime are better than the electrical drive based on the PI control. The ability to impose constraints on the next input move is the main advantage of MPC, as demonstrated by the simulation results presented in this paper.

6.2Recommendation

The thesis can also be extended to operate the motor at speeds higher than the rated speed; in the field weakening region. When the motor speed is extended beyond the base speed, a flux-weakening technique is used. Gain scheduled predictive control and removing the mechanical sensor are two areas for future research. Sensorless control (control with no rotor position sensor) is also possible. The relevant part of the unit circle stability boundary is also shown, and the eigenvalues, as expected, move toward the stability boundary as the speed increases, but the plot does show a measure of robustness in the control law design. This preliminary analysis lays the groundwork for further research into robustness. Constrained design, comparisons with PI controllers, and parameter uncertainties should all be included in such research.

REFERENCE

[1] F. Yusivar, N. Hidayat, R. Gunawan and A. Halim , "Implementation of Field Oriented Control for Permanent Magnet Synchronous Motor," in Electrical Engineering and Computer Science (ICEECS), pp. 359-362, 2014.

[2] Yue Zhao, “Position/speed sensorless control for permanent-magnet synchronous machines,” Electrical Engineering Theses and Dissertations University of Nebraska-Lincoln, Spring 4-2014.

[3] S. Chi, Z. Zhang, and L. Xu, “Sliding-mode sensorless control of direct-drive PM synchronous motors for washing machine applications,” IEEE Trans. Industry Applications, vol. 45, no. 2, pp. 582-590, Mar.-Apr. 2009.

[4] Pejcic, I.; Korda, M.; Jones, C.N. Control of nonlinear systems with explicit-MPC-like controllers. In Proceedings of the IEEE 56th Annual Conference on Decision and Control (CDC), Melbourne, VIC, Australia, 12-15 December 2017; pp. 4970-4975.

[5] Vazquez, S.; Aguilera, R.P.; Pablo Acuna, J.P.; Agelidis, V.G. Model Predictive Control for Single-Phase NPC Converters Based on Optimal Switching Sequences. IEEE Trans. Ind. Electron. 2016, 63, 7533-7543.

[6] Kakosimos, P.; Abu-Rub, H. Predictive Speed Control with Short Prediction Horizon for Permanent Magnet Synchronous Motor Drives. IEEE Trans. Power Electron. 2018, 33, 2740-2750.

[7] Rubino, S.; Bojoi, R.; Odhano, S.A.; Zanchetta, P. Model predictive direct flux vector control of multi three-phase induction motor drives. IEEE Trans. Ind. Appl. 2018.

[8] Zhang, Y.; Huang, L.; Xu, D.; Liu, J.; Jin, J. Performance evaluation of two-vector-based model predictive current control of PMSM drives. Chin. J. Electr. Eng. 2018, 4, 65-81.

[9] Zhang, X.; He, Y. Direct Voltage-Selection Based Model Predictive Direct Speed Control for PMSM Drives without Weighting Factor. IEEE Trans. Power Electron. 2018.

[10] F. Genduso, R. Miceli, C. Rando and G. R. Galluzzo, "Back-EMF Sensorless Control Algorithm for High Dynamics Performances PMSM, vol. 13, no. 05, pp. 1342- 1349, 2009.

[11] L. An, D. Franck, and K. Hameyer, "Sensorless field oriented control using back-EMF and flux observer for a surface mounted permanent magnet synchronous motor," International Journal of Applied Electromagnetic and Mechanics, vol. 45, no. 1-4, pp. 845-850, 2015.

[12] V. Nagarajan, M. Balaji and V. Kamaraj, "Back-Emf-Based Sensorless Field-Oriented control of PMSM using Neural-network-based controller with start-up strategy," Advance in Intellegent systems and Computing, vol. 325, pp. 449-457, 2015.

[13] B. Nahid-Mobarakeh, F. Meibody-Tabar and F. M. Sargos, "Back EMF estimation based sensorless control of PMSM: Robustness with respect to measurement errors and inverter irregularities," in Industry Applications control, vol. 34, no. 07, pp. 1231-1239, 2004.

[14] J. Beegum and Sema, " Comparision of Speed Control of PMSM with PI,PID and Adaptive PID controllers," IRJET, vol. 43, no. 05, pp. 1656-1667, 2016.

[15] J. K. J. Kang, B. H. B. Hu, H. L. H. Liu and G. X. G. Xu, "Sensorless Control of Permanent Magnet Synchronous Motor Based on Extended Kalman Filter," in 2009 IITA International Conference on Services Science, Management and Engineering, pp. 571- 574, 2009.

[16] J. Son and J. Lee, "A High-Speed Sliding-Mode Observer for the Sensorless Speed Control of a PMSM," IEEE Transactions On Industrial Electronics, vol. 58, no. 9, pp. 4069-4077, 2011.

[17] S. K. Kommuri, J. J. Rath, K. C. Veluvolu, M. Defoort, and S. Tatinati " Performance comparison of sliding mode observers for back EMFs based speed estimation in PMSM," International Conference on Control in Automation and Systems (ICCAS), 2015.

[18] Mahlet Legesse, " Speed Control of Vector Controlled PMSM Drive using Fuzzy LogicPI Controller." thesis for the degree of Master of Science in Electrical and Computer Engineering Addis Ababa Institute of Technology (AAiT), August, 2011.

[19] Derege Eskeza, "Speed control of permanent magnet synchronous motor using Higher order Sliding mode cotroller ," Msc thesis for the degree of Masters of science in electrical and computer Engineering Addis Abeba Institute of Technology (AAiT), 2017.

[20] Syed Abdul Rahman Kashif and Muhammad Asghar Saqib, "Sensorless Control of PMSM Drive is using Neural Network Observer," Electrical machines drive, Transaction on IEEE, pp. 1526-1533, 2016.

[21] Ji-Hoon Jang, “Sensorless Drive of Surface-Mounted Permanent-Magnet Motor by High Frequency Signal Injection Based on Magnetic Saliency,vol. 36, no. 15, pp. 1723-1726, 2003.

[22] D. Mayne et al. “Constrained model predictive control: Stability and optimality”. En: (2000).

[23] J. Rodriguez y P. Cort´es. Predictive Control of Power Converter and Electrical Drives. 2012.

[24] J. Rodr´ıguez et al P. Cort´es M. Kazmierkowski, “Predictive Control in Power Electronics and Drives”, En: (2008).

[25] Domenico Casadei, Fransesco Profumo, Giovanni Serra, Angelo Tani,, " Field Oriented Control and Direct Torque control of two viable schemes for induction motors torque control," IEEE Transactions on power Electronics, vol. 3, no. 06, pp. 219-227, 2017.

[26] M. Kazmierkowski et al J. Rodr´ıguez P. Cort´es. “State of the Art of Finite Control Set Model Predictive Control in Power Electronics”, En: (2011).

[27] Krishnan, R. Permanent Magnet Synchronous and Brushless DC Motor Drives; CRC Press/Taylor & Francis: Boca Raton, FL, USA, 2010,

[28] Rodriguez, J.; Pontt, J.; Silva, C.A.; Correa, P.; Lezana, P.; Cortes, P.; Ammann, U. Predictive Current Control of a Voltage Source Inverter. IEEE Trans. Ind. Electron. 2007, 54, 495-503.

[29] C. Yong, Z. Fu and L. Xia et al, "Online adaptive parameter identification of PMSM based on the dead-time compensation," International Journal of Electronics, vol. 102, no. 07, pp. 1132-1150, 2015.

APPEDIX-A

PARAMETERS OF PMSM

Table A.1 Motor Parameters for PMSM

parameter	Value	Parameter	Value
No of pole (P_n)	4	Friction coefficient (B)	0.008Nms
Stator Inductances (L_d and L_q)	5.25e-3H and 12e-3H	rotor inertia (J)	0.003JKgm²
Stator resistance (R)	0.958ohm	rotor flux linkage	0.1827Vs

APPENDIX - B

The code's primary function is to determine the states of MOSFETs based on the cost function g. If states S1, S2, and S3 are obtained, the entire state of all MOSFETs can be determined using the topology shown in Figure (3.4). States S4, S5 and S6 are diametrically opposed to the first three.

```
function [S1,S2,S3,S4,S5,S6]=
MPC(Wr,isd,isq,isq_ref,t,teta)

Ts=1e-5;
L=0.00153;
R=2.875;
Sim=0.175;
Vdc=500;
S=[0 0 0;0 0 1;0 1 0;0 1 1;1 0 0;1 0 1;1 1 0;1 1 1];
cost=zeros(8,1);
    S1=0;
    S2=0;
    S3=0;
    S4=0;
    S5=0;
    S6=0;
for i=1:1:8
    Sa=S(i,1);
    Sb=S(i,2);
    Sc=S(i,3);
    Vinva=(Vdc*(2*Sa-Sb-Sc))/3;
    Vinvb=(Vdc*(2*Sb-Sa-Sc))/3;
    Vinvc=(Vdc*(2*Sc-Sb-Sa))/3;
sq=(2/3)*((Vinva*cos((Wr*t+teta)))+(Vinvb*cos((Wr*t)+teta+
(4*pi/3)))+(Vinvc*cos((Wr*t)+teta+(2*pi/3))));
vsd=(2/3)*((Vinva*sin((Wr*t+teta)))+(Vinvb*sin((Wr*t)+teta
+(4*pi/3)))+(Vinvc*sin((Wr*t)+teta+(2*pi/3))));
    isd_p=((1-(R*Ts/L))*isd)+(Ts*Wr*isq)+(vsd*Ts/L);
    isq_p=((1-(R*Ts/L))*isq)-(Ts*Wr*isd)-
(Sim*Wr*Ts)+(vsq*Ts/L);

    cost(i,1)=((isd_p)*(isd_p))+((isq_ref-isq_p)*(isq_ref-
isq_p));
end

[~,index]=sort(cost);
```

```
if index(1,1)==1
    S1=0;
    S2=1;
    S3=0;
    S4=1;
    S5=0;
    S6=1;
end
if index(1,1)==2
    S1=0;
    S2=1;
    S3=0;
    S4=1;
    S5=1;
    S6=0;
end
if index(1,1)==3
    S1=0;
    S2=1;
    S3=1;
    S4=0;
    S5=0;
    S6=1;
end
if index(1,1)==4
    S1=0;
    S2=1;
    S3=1;
    S4=0;
    S5=1;
    S6=0;
end
if index(1,1)==5
    S1=1;
    S2=0;
    S3=0;
    S4=1;
    S5=0;
    S6=1;
end
if index(1,1)==6
    S1=1;
    S2=0;
```

```
    S3=0;
    S4=1;
    S5=1;
    S6=0;
end
if index(1,1)==7
    S1=1;
    S2=0;
    S3=1;
    S4=0;
    S5=0;
    S6=1;
end
if index(1,1)==8
    S1=1;
    S2=0;
    S3=1;
    S4=0;
    S5=1;
    S6=0;
end

end
```